IL-33 causes orofacial neuropathic pain via phosphorylation of GluN2B in the trigeminal spinal subnucleus caudalis

Yuki Kimura

Nihon University Graduate School of Dentistry
Major in Oral and Maxillofacial Surgery I
(Directors: Profs. Morio Tonogi and Masamichi Shinoda and
Assoc. prof. Yoshinori Hayashi)

Index

This thesis is composed of the following article and additional results in terms of the effects of intracisternal administration of IL-33 on the development of mechanical allodynia in the whisker pad skin in female mice. (Fig. 14):

Kimura Y, Hayashi Y, Hitomi S, Ikutame D, Urata K, Shibuta I, Sakai A, Ni J, Iwata K, Tonogi M, Shinoda M (2021) IL-33 induces orofacial neuropathic pain through Fyn-dependent phosphorylation of GluN2B in the trigeminal spinal subnucleus caudalis. Brain Behav Immun 99, 266-280.

Abstract

Neuropathic pain can cause considerable disruptions in patients' daily lives, especially because of a lack of effective medications as its underlying causative mechanisms are not fully understood. Here, I found neuron-specific expression of the interleukin (IL)-33 receptor in the trigeminal spinal subnucleus caudalis (Vc), distinct from the spinal dorsal horn. Reduction in head withdrawal threshold in response to von Frey filament stimulation of the whisker pad skin was inversely correlated with the upregulation of IL-33 in the Vc after infraorbital nerve injury (IONI). Neutralization of IL-33 in the Vc alleviated mechanical allodynia in the whisker pad skin after IONI; conversely, intracisternal administration of IL-33 elicited mechanical allodynia in the whisker pad skin, which was relieved by GluN2B antagonism. Furthermore, IL-33 triggered the facilitation of GluN2B-containing *N*-methyl-D-aspartate receptor-mediated synaptic currents and phosphorylation of synaptosomal GluN2B in the Vc, whereas IONI-induced GluN2B phosphorylation was inhibited by neutralization of IL-33 in the Vc. IL-33-produced GluN2B phosphorylation was mediated by phosphorylation of Fyn kinase, and inhibition of the Fyn kinase pathway prevented the development of IL-33-induced mechanical allodynia. IL-33-induced mechanical allodynia was also observed in female mice. These findings provide insights into a new mechanism by which IL-33 directly regulates synaptic transmission and suggest that IL-33 signaling could be a candidate target for therapeutic interventions for orofacial neuropathic pain.

Abbreviations

IL: interleukin

Vc: trigeminal spinal subnucleus caudalis

IONI: infraorbital nerve injury

SDH: spinal dorsal horn

SNI: spinal nerve injury

ST2: suppression of tumorigenicity 2

CNS: central nervous system

rhST2: recombinant human ST2

rhIL-33: recombinant human IL-33

NMDARs: *N*-methyl-D-aspartate receptors

SFKs: Src family kinases

HWT: head withdrawal threshold

PBS: phosphate-buffered saline

OLIG2: oligodendrocyte transcription factor 2

IBA1: ionized calcium-binding adapter molecule 1

GFAP: glial fibrillary acidic protein

SOX9: SRY-box transcription factor 9

NeuN: neuronal nuclei

MAP2: microtubule-associated protein 2

TBS-T: Tween-20 diluted in Tris-buffered saline

ACSF: artificial cerebrospinal fluid

mEPSCs: miniature excitatory postsynaptic currents

AMPARs: α-amino-3-hydroxy-5-methyl-4-isoxazolepropionic acid receptors

SEM: standard error of the mean

ANOVA: analysis of variance

GEE: generalized estimating equation

BDNF: derived brain-derived neurotrophic factor

TrkB: tropomyosin receptor kinase

LTP: long-term potentiation

CaMKII: calmodulin-dependent kinase II

TNF-α: tumor necrosis factor-α

IFN-γ : interferon-γ

Introduction

Chronic orofacial pain is one of the most debilitating pain conditions because it severely impairs basic daily activities such as talking and eating. Multiple diseases, craniofacial injury, or dental treatment can cause trigeminal nerve injury, which leads to orofacial neuropathic pain [1]. Several treatments are available; however, patients frequently experience insufficient therapeutic effects. Many studies have reported that activation of glial cells such as microglia and astrocytes is observed in the trigeminal spinal nucleus caudalis (Vc) and the spinal dorsal horn (SDH) after trigeminal nerve and spinal nerve injury (SNI), respectively. [2,3,4]. Nevertheless, distinctions in pain sensitivity between the orofacial region and other regions have been also reported in studies in humans. Repetitive nociceptive thermal stimulation of a certain intensity may produce habituation in the hands while leading to sensitization in the face [5]. Moreover, when the same intensity of stimulation is applied to the face and hand, the amygdala is more activated by face stimulation [6]. Supporting this evidence, mice studies have clarified distinct projection patterns and gene profiles in trigeminal ganglion and dorsal root ganglion neurons [7,8,9]. A distinct microcircuitry in the brainstem and the spinal cord level might contribute to nociception in the orofacial region and other regions; however, the details are not fully understood.

Interleukin (IL)-33 possesses a β-trefoil-fold in its C-terminal domain, a characteristic feature of the IL-1 family [10]. The best-known members of this family are IL-1β and IL-18; unlike them, IL-33 is constitutively expressed in the nucleus, where it functions as a repressor of nuclear factor-kappa B [11], and is thereby characterized as a chromatin-associated cytokine

[12]. In response to cellular injury and stress, IL-33 is released extracellularly and binds to its specific receptor—suppression of tumorigenicity 2 (ST2; also known as IL-1 receptor-like 1)—which in turn triggers inflammatory signaling in immune cells such as basophils, T cells, and mast cells [13]. Accumulating evidence indicates that IL-33 is abundantly expressed in the central nervous system (CNS) and is involved in neuroinflammatory processes as well as physiological brain functions [14,15,16]. However, although downstream IL-33 signaling in the CNS remains largely unclear, recent studies have highlighted the role of the IL-33/ST2 pathway in nociception. Subcutaneous injection of IL-33 into the hind paw elicited spontaneous pain [17], whereas an increase in the serum levels of IL-33 has been observed in several painful situations associated with inflammation [18,19]. It is also noteworthy that blockade of ST2 in the SDH ameliorates mechanical allodynia in the hind paw following sciatic nerve injury [20,21].

Thus, although the IL-33/ST2 pathway plays an essential role in both acute and chronic pain, the role of IL-33 in orofacial pain remains unclear. The purpose of this study was to examine whether IL-33, as a pain-related molecule, also contributes to neuropathic pain in the orofacial region. We also examined whether the IL-33 signaling is contributed to the induction of mechanical allodynia in female mice.

Materials and methods

Animals

A total of 207 male and 6 female C57BL/6J mice (6–7 weeks old) were purchased from Japan SLC (Hamamatsu, Japan). All mice were housed at a temperature of 23 ± 1 °C with a 12 h light/dark cycle under specific pathogen-free conditions and *ad libitum* access to food and water. All mice were acclimated to the experimenter and the experimental environment for 5 days to minimize stress. Animal experiments and care were conducted according to the protocols approved by the Animal Experimentation Committee of Nihon University (protocol number: AP19DEN036-1 and AP21DEN007-1) and the ethical guidelines of the International Association for the Study of Pain [22].

Surgical procedures

Mice were anesthetized using a mixture of 4 mg/kg midazolam (Sandoz, Tokyo, Japan), 0.75 mg/kg medetomidine (Zenoaq, Koriyama, Japan), and 5 mg/kg butorphanol (Meiji Seika Pharma, Tokyo, Japan). To make the model of orofacial neuropathic pain, mice were subjected to infraorbital nerve injury (IONI) in a manner similar to that described in a previous study [2]. Briefly, a small incision was made in the left buccal mucosa, and the infraorbital nerve was separated from the surrounding tissue. One-third of the infraorbital nerve bundle was tightly ligated using 5-0 silk (Natsume, Tokyo, Japan), and the incision was then sutured (IONI: n = 82 mice). In the sham-operated group, the incision was sutured without nerve ligation (Sham-IONI: n = 41 mice). For intracisternal administration, a cannula (SP-10; Natsume, Japan) was

carefully inserted through a hole drilled in the occipital bone, and the tip of the cannula was placed at the cisterna magna. Intracisternal administration of IL-33-induced mechanical allodynia in the whisker pad skin in mice (male: n = 8 mice, female: n = 3 mice). For establishing the SNI model (n = 3 mice), the left side of the L4 spinal nerve was transected as previously described [3]. In Sham-SNI mice (n = 3 mice), the incision was sutured without nerve transection. After surgery, mice were allowed to recover in cages with sterile bedding. Two to three mice were housed per cage.

Drug administration

Under anesthesia with 2% isoflurane inhalation, 5 μl of drug solution or vehicle was administered through the cannula using a 25 μl Hamilton syringe (Hamilton, USA) and a 30-gauge needle. Recombinant human ST2 (rhST2; 300 ng; R&D Systems, USA) or saline was administered on day 5 after IONI; recombinant human IL-33 (rhIL-33; 100 ng; Peprotech, USA) or saline was administered to naive mice. Ro 25-6981 (a specific antagonist of GluN2B subunit-containing *N*-methyl-$_{D}$-aspartate receptors [NMDARs]; 300 nmol; Cayman Chemicals, USA) or dimethylsulfoxide (0.1% in saline) was administered 5 h after intracisternal administration of rhIL-33. Saracatinib (an inhibitor of Src family kinases [SFKs]; 100 nmol; Chemscene, USA), fluorocitrate (a metabolic inhibitor of astrocytes; 100 fmol; Sigma-Aldrich, USA), minocycline (an inhibitor of microglial activation; 500 nmol; Sigma-Aldrich), or saline was administered 2 h before rhIL-33 administration.

For the intracisternal administraiton of rhIL-33 or saline in female mice, 5 μl of rhIL-33 (100 ng) was administered through the cannula using a 25 μl Hamilton syringe (Hamilton, USA) and a 30-gauge needle.

von Frey test

Mice were placed in a chamber made of wire mesh (6 × 6 × 6 cm) and allowed to freely move about for 0.5–1 h for habituation to the experimental environment once daily for 5 days. Mechanical stimulation was conducted in accordance with a previously described method [2] . Calibrated von Frey filaments (0.07, 0.16, 0.4, 0.6, 1.0, 1.4, and 2.0 g; North Coast Medical, USA) were then applied to the left whisker pad skin, and the head withdrawal threshold (HWT), defined as the lowest von Frey filament intensity that evoked nociceptive responses, such as head withdrawal or vocalization, in response to more than three out of five stimuli, was assessed for each mouse. The cut-off value was set as 2.0 g.

Rotarod test

An automated rotarod treadmill (3 cm diameter; UgoBasil, Comerio, Italy) was used to assess motor performance as previously described [3]. Rotarod tests were conducted before and 5 h after intracisternal administration of Ro25-6981 (300 nmol/5 μl, n = 3 mice) or saracatinib (100 nmol/5 μl, n = 3 mice) in naive mice. The rotation rate of the rod was set to 5 rpm. The time spent on the rod was measured, and the cut-off time was set to 300 s.

Immunohistochemistry

Mice were transcardially perfused with phosphate-buffered saline (PBS) followed by 4% paraformaldehyde under deep anesthesia with 5% isoflurane inhalation prior to IONI, 1–5 days after IONI, 5 days after SNI, or 5 h after IL-33 administration. The brainstem and spinal cord were excised, fixed in 4% paraformaldehyde overnight at 4 °C, and then placed in 30% sucrose for 48 h at 4°C. Vc and L4 spinal cord slices (30 μm thick) were prepared using a cryostat

(Tissue-Tek Polar; Sakura Finetek, Tokyo, Japan). Blocking was performed in 1% normal donkey serum (Jackson ImmunoResearch, USA), 1% bovine serum albumin (Proliant Biologicals, USA), and 0.4% Triton X-100 (Wako, Osaka, Japan) in 0.01 M PBS for 1 h at room temperature. Thereafter, the slices were incubated for 2 days at 4 °C with primary antibodies against IL-33 (mouse monoclonal, 1:500; Cat. No. GTX14709; GeneTex, USA), oligodendrocyte transcription factor 2 (OLIG2) (rabbit monoclonal, 1:500; Cat. No. ab109186; Abcam, USA; goat polyclonal, 1:500; Cat. No. AF2418; R&D Systems), ionized calcium-binding adapter molecule 1 (IBA1) (rabbit polyclonal, 1:5000; Cat. No. 019-19741; Wako or goat polyclonal, 1:1000; Cat. No. ab5076; Abcam), glial fibrillary acidic protein (GFAP) (rabbit polyclonal, 1:5000; Cat. No. Z0334; Dako, Glostrup, Denmark or mouse monoclonal, 1:2000; Cat. No. MAB360; Merck Millipore, USA), SRY-box transcription factor 9 (SOX9) (goat polyclonal, 1:1000; Cat. No. AF3075; R&D Systems), neuronal nuclei (NeuN) (mouse monoclonal, 1: 2000; Cat. No. MAB377; Merck Millipore or rabbite polyclonal, 1:1000; Cat. No. GTX16208; GeneTex), ST2 (rabbit polyclonal, 1:500; Cat. No. PA5-23316; Thermo Fisher Scientific, USA), phospho-Fyn (pFyn) (rabbit polyclonal, 1:100; Cat. No. SAB4503872; Sigma-Aldrich), or microtubule-associated protein 2 (MAP2) (mouse monoclonal, 1:1000; Cat. No. M9942; Sigma-Aldrich), or Homer 1 (goat polyclonal, 1:200; Cat. No. Af1270; Frontier Institute, Hokkaido, Japan). The slices were washed three times in PBS and then incubated for 2 h at 4 °C with secondary antibodies conjugated with Alexa Fluor 488 or Alexa Fluor 555 (1:1000 each; Thermo Fisher Scientific). After gentle washing with PBS, the slices were mounted in an anti-fading medium (PermaFluor Aqueous Mounting Medium, Thermo Fisher Scientific). Images were captured using LSM510 or LSM710 confocal laser microscopes (Carl Zeiss, Oberkochen, Germany) with 10× (numerical aperture: 0.30) and 20×

(numerical aperture: 0.75) objective lenses and a 63× (numerical aperture: 1.4) oil immersion lens or a BZ-9000 system (Keyence, Osaka, Japan) with a 20× (numerical aperture: 0.75) objective lens. For the counting of IL-33-positive and OLIG2-positive cells, the middle part of the Vc, where the 2nd branch of the trigeminal nerve terminates, was imaged using the BZ-9000 system. The region of interest was set in the surface layer of the Vc (160000–180000 μm^2), which was measured using ImageJ (NIH; http://rsbweb.nih.gov/ij/). Cells were counted using the Cell Counter plugin in ImageJ, and then the density per 10000 μm^2 was calculated. To analyze the fluorescence intensity of IBA1 and GFAP immunoreactivity, images were captured using an LSM510 confocal laser microscope and converted into binary images using ImageJ. The region occupied by the pixels within images (image size: 450 × 450 μm^2) was measured using ImageJ. Three slices from each mouse were stained, and the average value was calculated. Red fluorescence changed to magenta as required.

Western blotting

After behavioral testing, mice were deeply anesthetized using 5% isoflurane and then perfused transcardially with ice-cold saline. The Vc was excised as described below and stored at -80 ºC until use.

For IL-33 detection, the Vc was excised from mice on day 5 after sham operation or IONI and lysed in lysis buffer (10 mM Tris-HCl, pH 7.4, 150 mM NaCl, 1% Triton X-100, and 0.5% NP-40) supplemented with 1% protease inhibitor cocktail (Sigma-Aldrich).

To detect GluN2B phosphorylation, the Vc was excised 5 h after administration of saline or rhST2 in IONI mice on day 5 or 5 h after administration of saline, IL-33, saline and IL-33, or saracatinib and IL-33 in naive mice. For isolation of the synaptosomal fraction from the Vc,

samples were lysed in lysis buffer with 1% protease inhibitor cocktail and 1% phosphatase inhibitor (Nacalai Tesque, Kyoto, Japan) and then using the Syn-PER Synaptic Protein Extraction Reagent with 1% protease inhibitor cocktail and 1% phosphatase inhibitor (Nacalai Tesque, Kyoto, Japan) according to the manufacturer's protocol.

To detect Fyn kinase phosphorylation, the Vc was excised 5 h after intracisternal administration of saline, IL-33, saline and IL-33, or saracatinib and IL-33 in naïve mice and lysed in RIPA buffer (25 mM Tris-HCl, pH 7.4, 150 mM NaCl, 1 mM EDTA, 1% NP-40, and 5% glycerol) supplemented with 1% protease inhibitor cocktail and 1% phosphatase inhibitor. Protein concentrations were determined using a BCA assay kit (TaKaRa, Shiga, Japan). Cell lysates (100 μg) were then treated with Dynabeads protein G (Thermo Fisher Scientific) coupled with anti-Fyn antibody (2 μg, mouse monoclonal, Cat. No. sc-434; Santa Cruz, USA) or anti-Src antibody (2 μg, rabbit monoclonal, Cat. No. 2123; Cell Signaling Technology), and the antigen was eluted according to the manufacturer's protocol. For the control experiments, immunoprecipitation was conducted using mouse IgG (2 μg, Cat. No. sc-434; Santa Cruz) or rabbit IgG (2 μg, Cat. No. 3900; Cell Signaling). The entire volume of the eluates was subjected to electrophoresis.

Electrophoresis, transfer, and band detection

Proteins (10–20 μg) obtained from each sample were resuspended in 2 × Laemmli buffer supplemented with 2-mercaptoethanol, heat-denatured for 5 min, electrophoresed using a 4–20% Mini-PROTEAN TGX Precast Gel (Bio-Rad, Hercules, USA), and transferred onto a polyvinylidene difluoride membrane (Trans-Blot Turbo Transfer Pack, Bio-Rad). After transfer, the blots were blocked using TBS-T (0.2% Tween-20 diluted in Tris-buffered saline) containing

5% Blocking One (for IL-33 detection) (Nacalai Tesque, Kyoto, Japan) or 5% Blocking One-P (for detecting phosphorylation) (Nacalai Tesque) for 1 h at room temperature, and then incubated with primary antibodies diluted in TBS-T containing 5% Blocking One or Blocking One-P overnight at 4 °C. The primary antibodies used were: anti-IL-33 antibody (1:1000; GeneTex), anti-phospho-GluN2B (pGluN2B) antibody (rabbit polyclonal, 1:2000; Cat. No. 10009761; Cayman Chemical, USA), anti-GluN2B antibody (rabbit polyclonal, 1:2000; Cat. No. 4207; Cell Signaling, USA), anti-phospho Src (pTyr416) antibody (mouse monoclonal, 1:1000; Cat. No. 05-677; Merck Millipore), anti-Fyn antibody (1:1000; Santa Cruz), anti-Src antibody (1:1000; Cell Signaling), and anti-β-actin antibody (mouse monoclonal, 1:200; Cat. No. sc-69879; Santa Cruz). After washing with TBS-T three times for 5 min, the blots were incubated with horseradish peroxidase-conjugated anti-mouse or rabbit secondary antibodies (1:2000 each; Cat. Nos. NA931, NA934; Cytiva, USA) for 2 h at room temperature. Membrane-bound horseradish peroxidase-labeled secondary antibodies were detected using Western Lightning ELC Pro (PerkinElmer, USA) and an image analyzer (ChemiDocXRS system; Bio-Rad). The band intensity was quantified using ImageJ. The IL-33, pGluN2B, pTyr420, and pTyr416 band intensities were normalized to those of β-actin, GluN2B, Fyn, and Src, respectively.

Mice were deeply anesthetized using 5% isoflurane 5 h after intracisternal administration of saline or IL-33, followed by intracardiac perfusion with ice-cold cutting solution (234 mM sucrose, 2.5 mM KCl, 1.25 mM NaH_2PO_4, 10 mM $MgCl_2$, 0.5 mM $CaCl_2$, 25 mM $NaHCO_3$, and 11 mM glucose, saturated with 95% O_2/5% CO_2). The brainstem was quickly removed and placed in ice-cold oxygenated cutting solution. Transverse Vc slices (200 μm thick) were prepared using the LinearSlicer PRO7 (Dosaka, Kyoto, Japan) and then recovered in artificial

cerebrospinal fluid (ACSF; 125 mM NaCl, 2.5 mM KCl, 1.25 mM NaH_2PO_4, 2 mM $MgCl_2$, 1.6 mM $CaCl_2$, 10 mM glucose, and 25 mM $NaHCO_3$, saturated with 95% O_2/5% CO_2). After 30–60 min, a Vc slice was placed in a submerged chamber perfused with ACSF at a flow rate of 2–3 ml/min. Whole-cell patch-clamp recordings were obtained from lamina I-II neurons in the middle part of the Vc, where the 2nd branch of the trigeminal nerve terminates. Vc neurons were visually identified using an infrared-differential interference contrast microscope (BX51WI; Olympus, Japan) equipped with a 40× water-immersion objective lens. Patch electrodes (5–8 MΩ) were fabricated using a Sutter P-97 (Sutter Instruments, Novato, USA) from borosilicate glass (outer diameter: 1.5 mm, inner diameter: 1.17 mm; Harvard Apparatus, Holliston, USA). Pipettes were filled with internal solution composed of 105 mM Cs-methanesulfonate, 17.5 mM CsCl, 10 mM BAPTA, 10 mM HEPES, 5 mM QX-314, 2 mM MgATP, and 0.5 mM Na_2GTP, adjusted to pH 7.25. Voltage-clamp recordings were obtained using a Multiclamp 700B amplifier (Molecular Devices, USA), Digidata 1440A (Molecular Devices), and Clampex 10.7 (Molecular Devices). Signals were digitized at 10 kHz and low-pass filtered at 1 kHz. During the recording of miniature excitatory postsynaptic currents (mEPSCs), 500 nM tetrodotoxin, 10 μM Cd^{2+}, 10 μM strychnine, 10 μM bicuculline, and 50 μM 2,3-dioxo-6-nitro-1,2,3,4-tetrahydrobenzo[f]quinoxaline-7-sulfonamide were added to the ACSF to block voltage-gated Na^+ channel, voltage-gated Ca^{2+} channel, glycinergic, and γ-aminobutyric acid-ergic currents and α-amino-3-hydroxy-5-methyl-4-isoxazolepropionic acid receptor (AMPAR)-mediated mEPSCs, respectively. Membrane potential was initially held at -60 mV for a while, and then the holding potential was gradually adjusted to +60 mV for the removal of the Mg^{2+} blockade of NMDARs. Following the acquisition of NMDAR-mediated mEPSCs, ACSF containing Ro 25-6981 (1 μM) was perfused. NMDAR-mediated mEPSC

amplitude was analyzed using Clampfit 10.7 (Molecular Devices). The inhibition rate of Ro 25-6981 was calculated based on the mean amplitude of NMDAR-mediated mEPSCs before and after Ro 25-6981 treatment.

Statistical analyses

Reagent selection; behavioral testing, immunohistochemistry, Western blotting, and electrophysiology experiments; and statistical analyses were conducted separately and in a blinded manner. Data are presented as the median ± interquartile range or mean ± standard error of the mean (SEM), as appropriate. Data normality was assessed using the Shapiro–Wilk test. Statistical analyses were performed using two-way analysis of variance (ANOVA) followed by Tukey's test, one-way ANOVA followed by Tukey's test, the Kruskal–Wallis test followed by Dunn's test, or unpaired Student's *t*-test using GraphPad Prism 7 (GraphPad Software Inc., USA). Repeated measures of a nonparametric test were assessed using generalized estimating equations (GEE) method followed by Bonferroni's test [23] in SPSS version 28 (IBM, USA). Differences were considered significant at $P < 0.05$.

Results

IL-33 was upregulated in oligodendrocytes in the Vc after IONI

To investigate the possible involvement of IL-33 in orofacial neuropathic pain, I established a mouse model of IONI. Reduction in HWT in the ipsilateral side of the whisker pad skin could be observed from day 1 after IONI and lasted throughout the experimental period, whereas HWT in the sham-IONI group was unaffected after surgery (GEE followed by Bonferroni's test, $P < 0.001$, df = 1, Wald chi-square = 114.16; Fig. 1A). No significant differences in the HWT in the contralateral side of the whisker pad skin were observed between sham-IONI and IONI mice (GEE followed by Bonferroni's test, $P = 0.000$, df = 1, Wald chi-square = 1.000; Fig. 1B). The number of IL-33-positive cells was increased in the ipsilateral side of the Vc; this increase was inversely proportional to HWT after IONI compared to the changes in the sham operation group (two-way ANOVA, Sham-IONI vs. IONI, Surgery: $P < 0.05$, $F_{(1, 2)} = 479.9$, Time: $P < 0.0001$, $F_{(5, 10)} = 67.28$; Fig. 1C, ipsilateral). Furthermore, the amount of IL-33 in the Vc was significantly upregulated after IONI (unpaired *t*-test, $P < 0.05$, $t_{(6)} = 3.426$; Fig. 1D). In the contralateral side of the Vc, the number of IL-33-positive cells was also increased after IONI (two-way ANOVA, Sham vs. IONI, Surgery: $P < 0.01$, $F_{(1, 2)} = 508.8$, Time: $P < 0.0001$, $F_{(5, 10)} = 36.14$; Fig. 1C, contralateral). To analyze the expression patterns of IL-33 in the Vc, a double-staining experiment was conducted. In the contralateral side of the Vc, IL-33 immunofluorescence was colocalized with OLIG2 (a marker for oligodendrocytes) immunofluorescence (Fig. 2A, arrow), and some IL-33 immunofluorescence was observed to be surrounded by GFAP (a marker for astrocytes) immunofluorescence (Fig. 2B, arrowheads).

This adjacent pattern of IL-33 and GFAP immunofluorescence may be due to their different subcellular localizations, as IL-33 and GFAP are nuclear and intermediate filament proteins, respectively. Therefore, I tried to confirm whether IL-33 is localized in astrocytes using an antibody against SOX9 (a specific marker of astrocytic nuclei) [24,25]. IL-33 immunofluorescence did not overlap with SOX9 immunofluorescence (Fig. 2C), indicating that astrocytes do not express IL-33 in the Vc. Besides, IL-33 immunofluorescence was not merged with IBA1 or NeuN immunofluorescence (Fig. 2D and E). Similar to the contralateral side, IL-33 immunofluorescence in the ipsilateral side of the Vc was restricted to oligodendrocytes (Fig. 2F-J). The expression patterns of IL-33 in the Vc did not differ between sham-IONI mice and IONI mice (Figs. 2 and 3). These results indicate that IL-33 is preferentially expressed in oligodendrocytes in the Vc. Similar to the increase in the number of IL-33-positive cells, the number of OLIG2-positive cells in both the ipsilateral and contralateral sides of the Vc was significantly increased following IONI (two-way ANOVA, ipsilateral, Surgery: $P < 0.01$, $F_{(1, 2)} = 198.4$, Time: $P < 0.0001$, $F_{(5, 10)} = 59.15$; contralateral, Surgery: $P < 0.01$, $F_{(1, 2)} = 155.7$, Time: $P < 0.0001$, $F_{(5, 10)} = 18.76$; Fig. 4A and B). The ratio of IL-33-positive cells in oligodendrocytes was time-dependently increased in both ipsilateral and contralateral sides of the Vc following IONI (two-way ANOVA, ipsilateral, Surgery: $P < 0.01$, $F_{(1, 2)} = 383.4$, Time: $P < 0.0001$, $F_{(5, 10)} = 51.25$; contralateral, Surgery: $P < 0.01$, $F_{(1, 2)} = 349.5$, Time: $P < 0.0001$, $F_{(5, 10)} = 41.53$; Fig. 4C). On the other hand, the number of OLIG2-positive cells were unchanged by sham-IONI (Fig. 4B and C). Recent studies have indicated that some populations of astrocytes express OLIG2, and that oligodendrocytes transform into astrocytes after CNS injury [26,27]. However, no overlap between OLIG2 and GFAP immunofluorescence was observed in the Vc following IONI (Fig. 4D).

IL-33 is necessary and sufficient for mechanical allodynia in the orofacial region

To demonstrate the necessity of IL-33 for mechanical allodynia in the orofacial region, rhST2 (a decoy receptor that neutralizes IL-33) or saline was administered intracisternally on day 5 after IONI. The reduction in HWT following IONI was significantly abrogated by a single administration of rhST2, but not saline (GEE followed by Bonferroni's test, $P < 0.05$, df = 1, Wald chi-square = 5.855; Fig. 5A). To further address whether IL-33 is sufficient to induce mechanical allodynia in the whisker pad skin, rhIL-33 or saline was administered intracisternally into naive mice. HWT was markedly reduced 1 h after a single administration of rhIL-33 but not saline; moreover, the reduction in HWT could even be observed 48 h after rhIL-33 administration (GEE followed by Bonferroni's test, $P < 0.001$, df = 1, Wald chi-square = 202.453; Fig. 5B). These results suggest that the IL-33/ST2 pathway is required in the Vc for orofacial neuropathic pain.

ST2 is expressed in neurons in the Vc

To explore the mechanism underlying IL-33-induced mechanical allodynia in the whisker pad skin, I assessed the distribution of ST2 in the Vc. ST2 immunofluorescence overlapped exclusively with that of NeuN, but not of GFAP, IBA1, or OLIG2 immunofluorescence in the ipsilateral and contralateral sides of the Vc in IONI or sham-IONI mice (Fig. 6A-H and 7, arrows). These data indicate that ST2 was expressed in neurons in the Vc. However, previous studies have suggested the existence of ST2 in neurons as well as microglia and astrocytes in the SDH [20, 21]. To clarify the expression patterns of ST2 between the Vc and SDH, I investigated the L4 SDH immunohistochemically. On day 5 after surgery, immunofluorescence of ST2 in the ipsilateral side of the L4 SDH overlapped with NeuN immunofluorescence (SNI

mice: 66.60 ± 3.67 %; sham-SNI mice: 73.34 ± 4.38 %; Fig.6 I and M, arrowheads). Distinct from that in the Vc, ST2 immunofluorescence also overlapped with GFAP immunofluorescence in the ipsilateral side of the L4 SDH (SNI mice: 33.39 ± 3.67 %; Sham-SNI mice: 26.65 ± 4.38 %) (Fig. 6J and N, arrows), consistent with the previous report [20]. No ST2/IBA1 or ST2/OLIG2 double-positive cells were observed in the ipsilateral sides of the L4 SDH in either SNI or sham-SNI mice (Fig. 6K, L, O, and P). The expression patterns of ST2 in the contralateral side of the L4 SDH were the same as those on the ipsilateral side in both SNI and sham-SNI mice (Fig. 7). As in the Vc, the IL-33-expressing cells in both the contralateral and ipsilateral sides of the L4 SDH were restricted to oligodendrocytes (Fig. 8A, arrows). Further, no overlap between OLIG2 and GFAP immunofluorescence was observed in the ipsilateral side of the L4 SDH following SNI (Fig. 8B). Distinct from the Vc, the number of OLIG2-positive cells was unaltered in the SDH following SNI (Fig. 9).

To further verify the absence of ST2 in astrocytes and microglia in the Vc, I stained for GFAP and IBA1 in the Vc following intracisternal administration of saline or IL-33. No obvious change in the fluorescence intensity of GFAP and IBA1 in the Vc was observed between saline- and IL-33-administered mice (unpaired *t*-test, GFAP: $P = 0.5079$, $t_{(9)} = 0.6896$, IBA1: $P = 0.7070$, $t_{(9)} = 0.3880$; Fig. 10A-G). In addition, ST2 immunofluorescence did not overlap with GFAP and IBA1 immunofluorescence after intracisternal administration of IL-33 (Fig. 10D and G). I also analyzed the effects of fluorocitrate (a metabolic inhibitor of astrocytes) or minocycline (an inhibitor of microglial activation) on IL-33-induced mechanical allodynia. Intracisternal administration of IL-33-induced mechanical allodynia in the whisker pad skin was not inhibited by pretreatment with fluorocitrate or minocycline (Fig. 10H), indicating that IL-33 might act directly on neurons but not astrocytes and microglia in the Vc.

IL-33 triggers GluN2B phosphorylation in the Vc

Due to the analgesic effects of NMDAR antagonists such as MK-801 and ketamine, it is widely believed that the activation of NMDARs (ionotropic glutamate receptors) is a prominent change in neurons during neuropathic pain [3,28]. In particular, GluN2B subunit-containing NMDARs are essential components in neuropathic pain [29,30]. Thus, I hypothesized that GluN2B subunit-containing NMDARs in Vc neurons were activated by intracisternal administration of IL-33. To assess the possible involvement of GluN2B subunit-containing NMDARs in IL-33-induced mechanical allodynia in the whisker pad skin, I intracisternally administered Ro 25-6981 (a specific antagonist of GluN2B subunit-containing NMDARs) or vehicle 5 h after IL-33 administration (Fig. 11A). IL-33-induced mechanical allodynia in the whisker pad skin was significantly but temporarily ameliorated by Ro 25-6981, but not by vehicle (GEE followed by Bonferroni's test, $P < 0.05$, df = 1, Wald chi-square = 4.261; Fig. 11B). The rotarod test revealed that motor performance in mice was unaltered by intracisternal administration of Ro 25-6981 (Pre: 300 ± 0 s; Post: 300 ± 0 s, n = 3 mice), indicating that the recovery effect of Ro 25-6981 on mechanical allodynia was not attributed to sedation. The above data indicate that GluN2B subunit-containing NMDARs were activated by IL-33. It has been reported that the hyperfunctioning of GluN2B subunit-containing NMDARs in the SDH following peripheral nerve injury is attributed to the phosphorylation of GluN2B at Tyr1472 (pGluN2B) [29,30]. Therefore, I isolated the synaptosomal fraction from the Vc of saline- or IL-33-administered mice and analyzed the amount of synaptic pGluN2B. The relative amount of pGluN2B in the Vc of IL-33-administered mice was 1.77-fold higher than that in saline-administered mice (unpaired *t*-test, $P < 0.01$, $t_{(8)} = 3.618$; Fig. 11C). GluN2A and GluN2B are typical NMDAR subunits, and subunit-specific gating control has been clarified [31]. Using

the whole-cell patch-clamp technique, NMDAR-mediated mEPSCs were recorded in Vc slices obtained from mice 5 h after intracisternal administration of saline or IL-33. Bath application of Ro 25-6981 caused a slight reduction in the amplitude of NMDAR-mediated mEPSCs in the Vc of saline-administered mice (5.96 ± 1.55 %). In contrast, a marked reduction in the amplitude of NMDAR-mediated mEPSCs in the Vc of IL-33 administered mice was observed after Ro 25-69818 treatment (51.0 ± 2.77 %) (unpaired *t*-test, $P < 0.0001$, $t_{(32)} = 13.69$; Fig. 11D). I also examined the involvement of GluN2B-containing NMDARs in IONI-induced mechanical allodynia in the whisker pad skin. The reduction in HWT following IONI was significantly abrogated by a single administration of Ro 25-6981 but not saline (GEE followed by Bonferroni's test, $P < 0.001$, df = 1, Wald chi-square = 29.623; Fig. 11E). I further addressed whether IL-33 signaling-mediated GluN2B phosphorylation occurred in the Vc following IONI (Fig. 11F). The amount of pGluN2B in the synaptosomal fraction from the Vc prepared on day 5 of IONI was 1.57-fold higher than that from sham-operated mice, and this increase was blunted after intracisternal administration of rhST2 (one-way ANOVA, $P < 0.01$, $F_{(2,10)} = 9.605$; Fig. 11G).

IL-33 triggers GluN2B phosphorylation through Fyn phosphorylation

Fyn, a member of the SFKs, is known to cause phosphorylation of GluN2B at Tyr1472 [29,30]. To investigate the possible involvement of Fyn kinase in IL-33-induced GluN2B phosphorylation in the Vc, I examined the phosphorylation of Fyn kinase upon IL-33 administration. The activation of Fyn and Src is regulated by phosphorylation at Tyr420 and Tyr416, respectively [29,32]. I immunoprecipitated Fyn or Src from whole cell lysate of the Vc from saline- or IL-33-administered mice, followed by detection of phosphorylation levels

of Tyr420 or Tyr416 using anti-pSrc (Tyr416) antibody which can detect both pTyr420 for Fyn and pTyr416 for Src. IL-33 administration caused a significant increase in Fyn phosphorylation at Tyr420, which was prevented by pretreatment with saracatinib (a broad inhibitor of SFKs) (one-way ANOVA, $P < 0.001$, $F_{(2, 12)} = 11.25$; Fig. 12A, left). In contrast, Src phosphorylation at Tyr416 was unaffected by the intracisternal administration of IL-33 (one-way ANOVA, $P = 0.5265$, $F_{(2, 12)} = 0.6770$; Fig. 12A, right). I also immunoprecipitated cell lysate from the Vc from sham-IONI and IONI mice on day 5 after surgery. Phosphorylated levels of both Tyr420 and Tyr416 in the Vc of IONI mice were significantly higher than those in sham-IONI mice (Fyn: $P < 0.01$, $t_{(7)} = 3.867$; Src: $P < 0.05$, $t_{(8)} = 2.990$; Fig. 12B). Cell lysates were also immunoprecipitated with normal mouse IgG (for Fyn) or rabbit IgG (for Src); however, no signal for Fyn or Src was detected by anti-Fyn or anti-Src antibodies (Fig. 13). Immunohistochemical analyses revealed pFyn-positive puncta could be observed in dendritic shafts but not soma in the Vc following IL-33 administration and in combination with MAP2 or NeuN staining (Fig. 12C, arrowheads). In contrast, the signals in the Vc of saline-administered mice were very faint (Fig. 12C). To further clarify whether pFyn-positive puncta were located in the dendritic spine, I performed double staining for pFyn and Homer 1 (a marker of postsynaptic density). pFyn puncta were closely matched to Homer 1 puncta in the Vc of IL-33-administered mice (Fig. 12C, circles), implying that Fyn is activated at the synaptic site. Next, the possible requirement of the IL-33/ST2/Fyn pathway for GluN2B phosphorylation was investigated. The amount of pGluN2B in IL-33-administered mice was significantly reduced by pretreatment with saracatinib (unpaired *t*-test, $P < 0.05$, $t_{(8)} = 2.905$; Fig. 12D). I also assessed the requirement of the Fyn kinase pathway for IL-33-induced mechanical allodynia. Pretreatment with saracatinib prevented the development of mechanical

allodynia in the whisker pad skin following intracisternal administration of IL-33 (GEE followed by Bonferroni's test, $P < 0.001$, df = 1, Wald chi-square = 406.309; Fig. 12E). Saracatinib itself did not influence motor performance in naïve mice (Pre: 300 ± 0 s; Post: 300 ± 0 s, n = 3 mice).

IL-33 signaling in the Vc contributes to orofacial neuropathic pain in female mice

To evaluate the requirement of IL-33 signaling in female mice, rhIL-33 or saline was administered intracisternally into naive female mice. Intracisternal administration of IL-33 but not saline caused the reduction of HWT in naive mice ($P = 0.000$, GEE Wald chi-square = 49.830; Fig. 14).

Discussion

Several studies have demonstrated the importance of cytokines in neuropathic pain, especially in mechanisms in the SDH [3,33,34]. The importance of cytokines in neuropathic pain in the orofacial region has also been studied [35], but their role in the Vc is not fully understood. In this study, I demonstrated that IL-33 and ST2 are exclusively expressed in oligodendrocytes and neurons in the Vc, respectively. Mechanical allodynia following IONI was dramatically relieved by inhibition of the IL-33/ST2 pathway. Intracisternal administration of IL-33 triggered mechanical allodynia in the whisker pad skin of naive mice, which was ameliorated by Ro 25-6981. Mechanical allodynia caused by IONI was also ameliorated by Ro 25-6981. IL-33 was able to potentiate GluN2B-containing NMDAR-mediated synaptic currents and facilitate the phosphorylation of synaptosomal GluN2B. Inhibition of Fyn kinase in the Vc prevented the induction of IL-33-induced mechanical allodynia and GluN2B phosphorylation. The IL-33/ST2 pathway was also required for the development of mechanical allodynia in the whisker pad skin in female mice (Fig.14). These findings indicate that oligodendrocyte-derived IL-33 causes plastic changes in Vc neurons, culminating in orofacial neuropathic pain (Fig. 15).

The main difference between the Vc and SDH observed in this study was with regard to the expression pattern of ST2. In the past decade, *in vitro* experiments have revealed that both microglia and astrocytes possess *St2* mRNA [36]. Moreover, Zarpelon et al. found that intrathecal administration of IL-33 elicited an increase in protein levels of both IBA1 and GFAP in the SDH, which was abrogated by *St2* gene loss-of-function or pretreatment with

minocycline or fluorocitrate [21]. However, despite analysis using the same strain of mice used in the study by Zarpelon et al., ST2 expression was detected in both astrocytes and neurons in another study [20]. Nevertheless, both studies found that ST2 is expressed in astrocytes. On the other hand, whether ST2 is expressed in SDH microglia is open to debate because of the lack of experiments using microglia-specific *St2* knockout mice and histological analyses. Considering microglia-astrocyte communication [2,37], I cannot exclude the possibility that astrocyte-derived factors might activate microglia following intrathecal administration of IL-33. I also analyzed the expression pattern of ST2 in the SDH using the same antibody as in the study by Liu et al. [20] and found that ST2 was expressed in both astrocytes and neurons. Surprisingly, ST2 expression was restricted to neurons in the Vc, which is distinct from the SDH. In addition, no increase in the immunoreactivity of GFAP and IBA1 in the Vc was observed after intracisternal administration of IL-33, and no inhibitory effect of fluorocitrate on IL-33-induced mechanical allodynia in the whisker pad skin was observed. In contrast, IL-33-induced mechanical allodynia was partially inhibited by minocycline in 1 of 4 mice. Because minocycline has a direct protective effect on neurons [38], the effects of minocycline on Vc neurons cannot be ruled out. According to the expression patterns of ST2 in the Vc, ST2 is not expressed in microglia and astrocytes in the Vc. IL-33 expression has been observed in both oligodendrocytes and astrocytes [15,39,21]. In particular, IL-33 expression was found to be restricted to oligodendrocytes in the SDH in experiments that combined immunohistochemical analyses and *Il-33* knockout mice [15]. Oligodendrocyte-specific expression of IL-33 in the SDH has also been validated in IL-33/citrine reporter mice [21]. In line with previous reports, I found that IL-33 was exclusively expressed in oligodendrocytes in the SDH as well as the Vc, and that its expression did not overlap with that of SOX9 (astrocytic

nuclei), GFAP, IBA1, or NeuN. Taken together, these observations indicate that the IL-33/ST2 pathway in the Vc works differently from that in the SDH, which might contribute to the distinct pain sensitivities between the orofacial region and other regions.

It has been reported that GluN2B phosphorylation is observed in both neuropathic and inflammatory pain; however, distinct intracellular pathways lead to GluN2B phosphorylation [29,30,40]. Nerve injury triggers Fyn kinase-mediated GluN2B phosphorylation in the SDH [29], and microglia-derived brain-derived neurotrophic factor (BDNF) contributes to Fyn phosphorylation via tropomyosin receptor kinase B (TrkB) [30]. In contrast, inflammatory stimuli did not induce Fyn phosphorylation in the SDH [29], and GluN2B phosphorylation during inflammatory pain is elicited by ephrinB2-mediated activation of EphB [40]. GluN2B phosphorylation plays an important role in synaptic plasticity in both neuropathic and inflammatory pain. GluN2B phosphorylation at Tyr1472 strengthens the interaction between NMDAR and the postsynaptic density, which contains transmembrane receptors, scaffold proteins, and signaling molecules and plays an essential role in the induction of long-term potentiation (LTP), a representative form of synaptic plasticity [41,42,43]. LTP is also observed as a characteristic plastic change in nociceptive circuits in the SDH [44,45]. Another role of GluN2B is binding to Ca^{2+}/calmodulin-dependent kinase II (CaMKII) at the synapse, where CaMKII maintains its active form [46,47,48]. Accordingly, GluN2B phosphorylation is indispensable for synaptic plasticity and contributes to long-lasting pain. Moreover, a recent study clarified the direct role of IL-33 in neurons—it was shown to promote synapse formation in cultured hippocampal neurons, and intracerebroventricular administration of recombinant ST2 inhibited synaptic plasticity in hippocampal CA1 pyramidal neurons [26]. Considering the effects of IL-33 on synapse formation, I could not eliminate the possibility of changes in spine

density in Vc neurons following intracisternal administration of IL-33. Since IL-33 phosphorylated GluN2B in the synaptosomal fraction and potentiated GluN2B-containing NMDAR-mediated mEPSCs, at least in my study, IL-33 is likely to produce plastic changes through the activation of GluN2B in the Vc. These findings suggest that the analgesic effect of rhST2 might be attributed to the erasure of undesirable plastic changes that had occurred in the Vc microcircuitry. The current results highlight the importance of NMDARs in the IL-33 pathway. However, I could not deny the involvement of AMPAR in the IL-33 pathway. Chen et al. found that Ca^{2+}-permeable AMPAR-mediated currents were enhanced in the spinal neurons of rats with diabetic neuropathic pain [49], indicating that IL-33 may facilitate AMPAR-mediated currents during neuropathic pain. Further study is needed to clarify the effect of IL-33 on AMPARs. In addition to the direct effects of cytokines, including IL-1β, IL-6, and tumor necrosis factor-α (TNF-α) on neurotransmission [50], to the best of my knowledge, I have demonstrated for the first time that IL-33 also directly regulates synaptic transmission.

Nevertheless, the mechanisms underlying the upregulation of IL-33 are unclear. As mentioned above, IL-33 expression is restricted to oligodendrocytes in the SDH [15,21]. However, some IL-33-positive cells were negative for OLIG2. Although OLIG2 is expressed in all oligodendrocytes regardless of their developmental state [51], in rare instances, OLIG2-negative oligodendrocytes have been observed [52,53]. A recent study clarified that OLIG2-positive astrocytes are found in the brain [26]. In addition, oligodendrocytes are known to convert into astrocytes following CNS injury [54]. However, OLIG2 immunofluorescence was not colocalized with GFAP immunofluorescence in the Vc following IONI. This suggests that IL-33 is unlikely to be expressed except in oligodendrocytes in the Vc. Considering these facts,

some IL-33 might be expressed in OLIG2-negative oligodendrocytes. However, I could not evaluate the role of IL-33-positive/OLIG2-negative cells because of technical limitations, namely the lack of specific markers for OLIG2-negative oligodendrocytes. Rather surprisingly, I found an increase in the number of IL-33-positive oligodendrocytes even in the contralateral side of the Vc following IONI. However, the contralateral side of the whisker pad skin did not exhibit mechanical allodynia after IONI. Considering that intracisternal administration of IL-33 evoked mechanical allodynia in the whisker pad skin, IL-33 was likely released from oligodendrocytes in the ipsilateral but not contralateral side of the Vc following IONI. The underlying mechanisms for the increase in the number of oligodendrocytes in the Vc remain to be clarified. However, I considered the following potential mechanisms. Research has indicated that peripheral nerve injury leads to dysfunction of the descending inhibitory system that projects bilaterally to the SDH and Vc [55]. Since catecholamines have an inhibitory effect on the proliferation of oligodendrocyte progenitor cells [56], the reduced function of the descending inhibitory modulation may eliminate the inhibitory tone of constitutive oligodendrocyte proliferation. Given that oligodendrocyte progenitor cells are present not only in the developmental stage but also in the adult CNS [57], oligodendrocyte progenitor cells in the Vc may have proliferated bilaterally after IONI. On the other hand, no proliferation of oligodendrocytes was observed in the SDH after SNI. Since microglia are the only proliferative cells found in the SDH after nerve injury [58], unknown factors may be upregulated in the Vc after nerve injury distinct from the SDH. Further analysis is needed to elucidate the mechanism of oligodendrocyte proliferation in the Vc.

It is also unclear how IL-33 levels increase after IONI. A marked increase in IL-33-positive cells was detected in the Vc one day after IONI. The time course of the increase in the

number of IL-33-positive cells was analogous to that of microglial activation in the SDH and Vc after peripheral nerve injury [3,4,59]. The details of microglia-oligodendrocyte crosstalk during orofacial neuropathic pain remain unclear; however, microglia presumably influence the activation state of oligodendrocytes, because it has been reported that established neuropathic pain is not relieved by pharmacological inhibition or genetic ablation of microglia, which play an essential role in the induction phase of neuropathic pain [60]; in contrast, inhibition of ST2 signaling ameliorated established neuropathic pain. Considering the above evidence, it is conceivable that signal relay from microglia to oligodendrocytes is required for a phase shift from the induction phase to the chronic phase of pain. Several factors, such as interferon-γ (IFN-γ), IL-1β, TNF-α, and reactive oxygen species (ROS), have been identified as being responsible for microglia-oligodendrocyte crosstalk [61]. Among these molecules, IFN-γ and ROS possibly induce IL-33 in oligodendrocytes according to experiments in keratinocytes and bronchial epithelial cells, respectively [62]. The proliferation of oligodendrocytes is regulated by IL-1β and TNF-α [63,64]. Accordingly, microglia-derived factors may influence oligodendrocyte function and promote IL-33 secretion.

Since saracatinib is a broad-spectrum SFK inhibitor, the possible involvement of SFKs other than Fyn in IL-33-induced mechanical allodynia cannot be ruled out. Five SFKs—Src, Fyn, Yes, Lck, and Lyn—are expressed in the mammalian CNS [32] and have been identified as components of the NMDAR complex [65,66,67]. Fyn and Src induce selective phosphorylation of GluN2B and GluN2A, respectively [68]. However, Yes, Lck, and Lyn have not been reported to affect GluN2B phosphorylation. IL-33 caused selective phosphorylation of Fyn, but not Src, in the Vc, and saracatinib suppressed IL-33-induced GluN2B phosphorylation. Interestingly, Fyn phosphorylation has been observed in excitatory synapses

after IL-33 stimulation. In terms of synaptic plasticity, both induction and maintenance of LTP were markedly impaired in *Fyn*- but not *Src*-mutant mice [69]. As mentioned above, both microglia-derived BDNF and oligodendrocyte-derived IL-33 can independently phosphorylate Fyn kinase. The effect of saracatinib on IONI could not be examined, because the IL-33/ST2/Fyn pathway has not been rigorously evaluated in the presence of the BDNF/TrkB/Fyn pathway (microglia-neuron signaling) [30,70]. Given the selective phosphorylation of Fyn by IL-33, the inhibitory effect of saracatinib on IL-33-induced mechanical allodynia was presumably mediated by the suppression of Fyn kinase.

My results show that mechanical allodynia caused by IL-33 involves a common pathway in both male and female mice. Studies have indicated that microglia during neuropathic pain are sexually dimorphic, and that a microglia-dependent pathway is utilized in male but not female mice [71]. BDNF is a representative molecule released from microglia in male mice [70] and is involved in the phosphorylation of Fyn kinase [30]. Considering these findings, BDNF and IL-33 act synergistically to phosphorylate Fyn kinase in male mice, culminating in plastic changes in Vc neurons. In female mice, IL-33 but not BDNF contributes to the phosphorylation of Fyn kinase.

Conclusions

Oligodendrocyte-derived IL-33 induces Fyn phosphorylation, ultimately leading to GluN2B phosphorylation in Vc neurons after IONI, and GluN2B-containing NMDARs in the synaptic site being activated by IL-33. Moreover, inhibition of the IL-33/ST2 pathway alleviated mechanical allodynia. Thus, IL-33 induces a plastic change in Vc neurons following IONI, resulting in the development of orofacial neuropathic pain. It has been proposed that cell-cell interactions, such as microglia-neuron, astrocyte-neuron, and microglia-astrocyte interactions, are involved in neuropathic pain [2, 32] and cooperatively facilitate the development of orofacial neuropathic pain. In addition to this, I propose that oligodendrocyte-neuron interactions via IL-33 signaling have an important role in orofacial neuropathic pain in male and female mice. My results suggest the existence of a new mechanism by which orofacial neuropathic pain is segregated from bodily pain, and may lead to the development of therapeutic strategies based on oligodendrocyte-neuron communication.

Acknowledgments

I am grateful to Prof. Tonogi for giving the opportunity to this study, Prof. Shinoda and Assoc. Prof. Hayashi for their experimental guidance of this study. I also thank colleagues in the Department of Oral and Maxillofacial Surgery I for their support and colleagues in Department of Physiology for their technical advice and assistance.

References

1. Penarrocha M, Cervello MA, Marti E, Bagan JV (2007) Trigeminal neuropathy. Oral Dis., 13(2): 141-50.
2. Asano S, Hayashi Y, Iwata K, Shibuta I, Imamura Y, Shinoda M et al (2020) Microglia-astrocyte communication via c1q contributes to orofacial neuropathic pain associated with infraorbital nerve injury. Int. J. Mol. Sci., 21(18): 6834.
3. Hayashi Y, Kawaji K, Sun L, Zhang X, Koyano K, Yokoyama T (2011) Microglial Ca(2+)-activated K(+) channels are possible molecular targets for the analgesic effects of S-ketamine on neuropathic pain. J. Neurosci., 31(48): 17370-82.
4. Tsuda M, Shigemoto-Mogami Y, Koizumi S, Mizokoshi A, Kohsaka S, Salter MW (2003) P2X4 receptors induced in spinal microglia gate tactile allodynia after nerve injury. Nature, 424(6950): 778-83.
5. Schmidt K, Schunke O, Forkmann K, Bingel U (2015) Enhanced short-term sensitization of facial compared with limb heat pain. J. Pain, 16(8): 781-90.
6. Moulton EA, Pendse G, Morris S, Strassman A, Aiello-Lammens M, Becerra L (2007) Capsaicin-induced thermal hyperalgesia and sensitization in the human trigeminal nociceptive pathway: an fMRI study. Neuroimage, 35(4): 1586-600.
7. Megat S, Ray PR, Tavares-Ferreira D, Moy JK, Sankaranarayanan I, Wanghzou A (2019) Differences between Dorsal Root and Trigeminal Ganglion Nociceptors in Mice Revealed by Translational Profiling. J. Neurosci., 39(35): 6829-47.

8. Rodriguez E, Sakurai K, Xu J, Chen Y, Toda K, Zhao S (2017) A craniofacial-specific monosynaptic circuit enables heightened affective pain. Nat. Neurosci., 20(12): 1734-43.
9. Shiratori-Hayashi M, Hasegawa A, Toyonaga H, Andoh T, Nakahara T, Kido-Nakahara M (2019) Role of P2X3 receptors in scratching behavior in mouse models. J. Allergy Clin. Immunol., 143(3): 1252-4 e8.
10. Schmitz J, Owyang A, Oldham E, Song Y, Murphy E, McClanahan TK (2005) IL-33, an interleukin-1-like cytokine that signals via the IL-1 receptor-related protein ST2 and induces T helper type 2-associated cytokines. Immunity, 23(5): 479-90.
11. Ali S, Mohs A, Thomas M, Klare J, Ross R, Schmitz ML (2011) The dual function cytokine IL-33 interacts with the transcription factor NF-kappaB to dampen NF-kappaB-stimulated gene transcription. J. Immunol., 187(4): 1609-16.
12. Carriere V, Roussel L, Ortega N, Lacorre DA, Americh L, Aguilar L et al (2007) IL-33, the IL-1-like cytokine ligand for ST2 receptor, is a chromatin-associated nuclear factor in vivo. Proc. Natl. Acad. Sci. U. S. A., 104(1): 282-7.
13. Liew FY, Girard JP, Turnquist HR (2016) Interleukin-33 in health and disease. Nat. Rev. Immunol., 16(11): 676-89.
14. Dohi E, Choi EY, Rose IVL, Murata AS, Chow S, Niwa M (2017) Behavioral Changes in Mice Lacking Interleukin-33. eNeuro, 4(6).
15. Gadani SP, Walsh JT, Smirnov I, Zheng J, Kipnis J (2015) The glia-derived alarmin IL-33 orchestrates the immune response and promotes recovery following CNS injury. Neuron, 85(4): 703-9.

16. Schmitz J, Owyang A, Oldham E, Song Y, Murphy E, McClanahan TK (2005) IL-33, an interleukin-1-like cytokine that signals via the IL-1 receptor-related protein ST2 and induces T helper type 2-associated cytokines. Immunity, 23(5): 479-90.

17. Verri WA, Jr. Guerrero AT, Fukada SY, Valerio DA, Cunha TM, Xu D et al (2008) IL-33 mediates antigen-induced cutaneous and articular hypernociception in mice. Proc. Natl. Acad. Sci. U. S. A., 105(7): 2723-8.

18. Gomez Lopez M, Dominguez Lopez A, Abarca Rojano E, Rojas Hernandez S, Martinez Godinez Mde L, Miliar Garcia A et al (2015) 17beta-Estradiol transcriptionally modulates Nlrp1 and Nlrp3 inflammasomes in gonadectomized rats with inflammation. Immunopharmacol. Immunotoxicol., 37(4): 343-50.

19. Xu D, Jiang HR, Kewin P, Li Y, Mu R, Fraser AR (2008) IL-33 exacerbates antigen-induced arthritis by activating mast cells. Proc. Natl. Acad. Sci. U. S. A., 105(31): 10913-8.

20. Liu S, Mi WL, Li Q, Zhang MT, Han P, Hu S et al (2015) Spinal IL-33/ST2 Signaling Contributes to Neuropathic Pain via Neuronal CaMKII-CREB and Astroglial JAK2-STAT3 Cascades in Mice. Anesthesiology, 123(5): 1154-69.

21. Zarpelon AC, Rodrigues FC, Lopes AH, Souza GR, Carvalho TT, Pinto LG et al (2016) Spinal cord oligodendrocyte-derived alarmin IL-33 mediates neuropathic pain. FASEB J., 30(1): 54-65.

22. Zimmermann M (1983) Ethical guidelines for investigations of experimental pain in conscious animals. Pain, 16(2): 109-10.

23. Ballinger GA (2004) Using generalized estimating equations for longitudinal data analysis. Organ Res Methods, 7(2): 127-50.

24. Sun W, Cornwell A, Li J, Peng S, Osorio MJ, Aalling N (2017) SOX9 Is an Astrocyte-Specific Nuclear Marker in the Adult Brain Outside the Neurogenic Regions. J. Neurosci., 37(17): 4493-507.

25. Tsuda M, Kohro Y, Yano T, Tsujikawa T, Kitano J, Tozaki-Saitoh H et al (2011) JAK-STAT3 pathway regulates spinal astrocyte proliferation and neuropathic pain maintenance in rats. Brain, 134(Pt 4): 1127-39.

26. Wang H, Xu L, Lai C, Hou K, Chen J, Guo Y (2021) Region-specific distribution of Olig2-expressing astrocytes in adult mouse brain and spinal cord. Mol. Brain, 14(1): 36.

27. Xianshu Bai NZ, Wenhui Huang Laura C. Caudal Renping Zhao, Johannes Hirrlinger, Wolfgang Walz, Frank Kirchhoff, Anja Scheller (2021) After traumatic brain injury oligodendrocytes regain a plastic phenotype and can become astrocytes. bioRxiv.

28. Seltzer Z, Cohn S, Ginzburg R, Beilin B (1991) Modulation of neuropathic pain behavior in rats by spinal disinhibition and NMDA receptor blockade of injury discharge. Pain, 45(1): 69-75.

29. Abe T, Matsumura S, Katano T, Mabuchi T, Takagi K, Xu L (2005) Fyn kinase-mediated phosphorylation of NMDA receptor NR2B subunit at Tyr1472 is essential for maintenance of neuropathic pain. Eur. J. Neurosci., 22(6): 1445-54.

30. Hildebrand ME, Xu J, Dedek A, Li Y, Sengar AS, Beggs S (2016) Potentiation of Synaptic GluN2B NMDAR Currents by Fyn Kinase Is Gated through BDNF-Mediated Disinhibition in Spinal Pain Processing. Cell Rep., 17(10): 2753-65.

31. Vicini S, Wang JF, Li JH, Zhu WJ, Wang YH, Luo JH (1998) Functional and pharmacological differences between recombinant N-methyl-D-aspartate receptors. J. Neurophysiol., 79(2): 555-66.

32. Salter MW, Kalia LV (2004) Src kinases: a hub for NMDA receptor regulation. Nat. Rev. Neurosci., 5(4): 317-28.
33. Inoue K, Tsuda M (2018) Microglia in neuropathic pain: cellular and molecular mechanisms and therapeutic potential. Nat. Rev. Neurosci., 19(3): 138-52.
34. Kawasaki Y, Zhang L, Cheng JK, Ji RR (2008) Cytokine mechanisms of central sensitization: distinct and overlapping role of interleukin-1beta, interleukin-6, and tumor necrosis factor-alpha in regulating synaptic and neuronal activity in the superficial spinal cord. J. Neurosci., 28(20): 5189-94.
35. Shinoda M, Kubo A, Hayashi Y, Iwata K (2019) Peripheral and Central Mechanisms of Persistent Orofacial Pain. Front. Neurosci., 131227.
36. Yasuoka S, Kawanokuchi J, Parajuli B, Jin S, Doi Y, Noda M (2011) Production and functions of IL-33 in the central nervous system. Brain Res., 13858-17.
37. Miyoshi K, Obata K, Kondo T, Okamura H, Noguchi K (2008) Interleukin-18-mediated microglia/astrocyte interaction in the spinal cord enhances neuropathic pain processing after nerve injury. J. Neurosci., 28(48): 12775-87.
38. Tikka T, Fiebich BL, Goldsteins G, Keinanen R, Koistinaho J (2001) Minocycline, a tetracycline derivative, is neuroprotective against excitotoxicity by inhibiting activation and proliferation of microglia. J. Neurosci., 21(8): 2580-8.
39. Gadani SP, Walsh JT, Smirnov I, Zheng J, Kipnis J (2015) The glia-derived alarmin IL-33 orchestrates the immune response and promotes recovery following CNS injury. Neuron, 85(4): 703-9.

40. Vainchtein ID, Chin G, Cho FS, Kelley KW, Miller JG, Chien EC (2018) Astrocyte-derived interleukin-33 promotes microglial synapse engulfment and neural circuit development. Science, 359(6381): 1269-73.
41. Slack S, Battaglia A, Cibert-Goton V, Gavazzi I (2008) EphrinB2 induces tyrosine phosphorylation of NR2B via Src-family kinases during inflammatory hyperalgesia. Neuroscience, 156(1): 175-83.
42. Abraham WC (2008) Metaplasticity: tuning synapses and networks for plasticity. Nat. Rev. Neurosci., 9(5): 387.
43. Nakazawa T, Komai S, Tezuka T, Hisatsune C, Umemori H, Semba K (2001) Characterization of Fyn-mediated tyrosine phosphorylation sites on GluR epsilon 2 (NR2B) subunit of the N-methyl-D-aspartate receptor. J. Biol. Chem., 276(1): 693-9.
44. Rong Y, Lu X, Bernard A, Khrestchatisky M, Baudry (2001) Tyrosine phosphorylation of ionotropic glutamate receptors by Fyn or Src differentially modulates their susceptibility to calpain and enhances their binding to spectrin and PSD-95. J. Neurochem., 79(2): 382-90.
45. Ikeda H, Heinke B, Ruscheweyh R, Sandkuhler J (2003) Synaptic plasticity in spinal lamina I projection neurons that mediate hyperalgesia. Science, 299(5610): 1237-40.
46. Kronschlager MT, Drdla-Schutting R, Gassner M, Honsek SD, Teuchmann HL, Sandkuhler J (2016) Gliogenic LTP spreads widely in nociceptive pathways. Science, 354(6316): 1144-8.
47. Barcomb K, Hell JW, Benke TA, Bayer KU (2016) The CaMKII/GluN2B Protein Interaction Maintains Synaptic Strength. J. Biol. Chem., 291(31): 16082-9.

48. Bayer KU, De Koninck P, Leonard AS, Hell JW, Schulman H (2001) Interaction with the NMDA receptor locks CaMKII in an active conformation. Nature, 411(6839): 801-5.

49. Halt AR, Dallapiazza RF, Zhou Y, Stein IS, Qian H, Juntti S et al 2012. CaMKII binding to GluN2B is critical during memory consolidation. EMBO J., 31(5): 1203-16.

50. Chen SR, Zhang J, Chen H, Pan HL (2019) Streptozotocin-Induced Diabetic Neuropathic Pain Is Associated with Potentiated Calcium-Permeable AMPA Receptor Activity in the Spinal Cord. J. Pharmacol. Exp. Ther., 371(2): 242-9.

51. Kawasaki Y, Zhang L, Cheng JK, Ji RR (2008) Cytokine mechanisms of central sensitization: distinct and overlapping role of interleukin-1beta, interleukin-6, and tumor necrosis factor-alpha in regulating synaptic and neuronal activity in the superficial spinal cord. J. Neurosci., 28(20): 5189-94.

52. Zhou B, Zhu Z, Ransom BR, Tong X (2021) Oligodendrocyte lineage cells and depression. Mol. Psychiatry, 26(1): 103-17.

53. Han R, Yang YM, Dietrich J, Luebke A, Mayer-Proschel M, Noble M (2008) Systemic 5-fluorouracil treatment causes a syndrome of delayed myelin destruction in the central nervous system. J. Biol., 7(4): 12.

54. Kleopa KA, Sargiannidou I, Markoullis K (2013) Connexin pathology in chronic multiple sclerosis and experimental autoimmune encephalomyelitis. Clinical and Experimental Neuroimmunology, 445-58.

55. Xianshu Bai NZ, Wenhui Huang Laura C. Caudal Renping Zhao, Johannes Hirrlinger, Wolfgang Walz, Frank Kirchhoff, Anja Scheller (2021) After traumatic brain injury oligodendrocytes regain a plastic phenotype and can become astrocytes. bioRxiv.

56. Ghiani CA, Eisen AM, Yuan X, DePinho RA, McBain CJ, Gallo V (1999) Neurotransmitter receptor activation triggers p27(Kip1)and p21(CIP1) accumulation and G1 cell cycle arrest in oligodendrocyte progenitors. Development, 126(5): 1077-90.

57. Young KM, Psachoulia K, Tripathi RB, Dunn SJ, Cossell L, Attwell D et al (2013) Oligodendrocyte dynamics in the healthy adult CNS: evidence for myelin remodeling. Neuron, 77(5): 873-85.

58. Gu N, Peng J, Murugan M, Wang X, Eyo UB, Sun D et al(2016) Spinal Microgliosis Due to Resident Microglial Proliferation Is Required for Pain Hypersensitivity after Peripheral Nerve Injury. Cell Rep., 16(3): 605-14.

59. Shibuta K, Suzuki I, Shinoda M, Tsuboi Y, Honda K, Shimizu N et al(2012) Organization of hyperactive microglial cells in trigeminal spinal subnucleus caudalis and upper cervical spinal cord associated with orofacial neuropathic pain. Brain Res., 145174-

60. Peng J, Gu N, Zhou L, U BE, Murugan M, Gan WB (2016) Microglia and monocytes synergistically promote the transition from acute to chronic pain after nerve injury. Nat Commun, 712029.

61. Peferoen L Kipp M, van der Valk P, van Noort JM, Amor S, (2014) Oligodendrocyte-microglia cross-talk in the central nervous system. Immunology, 141(3): 302-13.

62. Fujita T, Matsuoka T, Honda T, Kabashima K, Hirata T, Narumiya S (2011) A GPR40 agonist GW9508 suppresses CCL5, CCL17, and CXCL10 induction in keratinocytes and attenuates cutaneous immune inflammation. J. Invest. Dermatol., 131(8): 1660-7.

63. Arnett HA, Mason J, Marino M, Suzuki K, Matsushima GK, Ting JP (2001) TNF alpha promotes proliferation of oligodendrocyte progenitors and remyelination. Nat. Neurosci., 4(11): 1116-22.

64. Vela JM, Molina-Holgado E, Arevalo-Martin A, Almazan G, Guaza C (2002) Interleukin-1 regulates proliferation and differentiation of oligodendrocyte progenitor cells. Mol. Cell. Neurosci., 20(3): 489-502.

65. Kalia LV, Salter MW (2003) Interactions between Src family protein tyrosine kinases and PSD-95. Neuropharmacology, 45(6): 720-8.

66. Yaka R, Thornton C, Vagts AJ, Phamluong K, Bonci, A., Ron (2002) NMDA receptor function is regulated by the inhibitory scaffolding protein, RACK1. Proc. Natl. Acad. Sci. U. S. A., 99(8): 5710-5.

67. Yu M, Askalan R, Keil GJ, 2nd Salter MW (1997) NMDA channel regulation by channel-associated protein tyrosine kinase Src. Science, 275(5300): 674-8.

68. Yang K, Trepanier C, Sidhu B, Xie YF, Li H, Lei G (2012) Metaplasticity gated through differential regulation of GluN2A versus GluN2B receptors by Src family kinases. EMBO J., 31(4): 805-16.

69. Grant SG, O'Dell TJ, Karl KA, Stein PL, Soriano P, Kandel ER (1992) Impaired long-term potentiation, spatial learning, and hippocampal development in fyn mutant mice. Science, 258(5090): 1903-10.

70. Coull JA, Beggs S, Boudreau D, Boivin D, Tsuda M, Inoue K et al (2005) BDNF from microglia causes the shift in neuronal anion gradient underlying neuropathic pain. Nature, 438(7070): 1017-21.

71. Sorge RE, Mapplebeck JC, Rosen S, Beggs S, Taves S, Alexander JK et al. (2015) Different immune cells mediate mechanical pain hypersensitivity in male and female mice. Nat. Neurosci., 18(8): 1081-3.

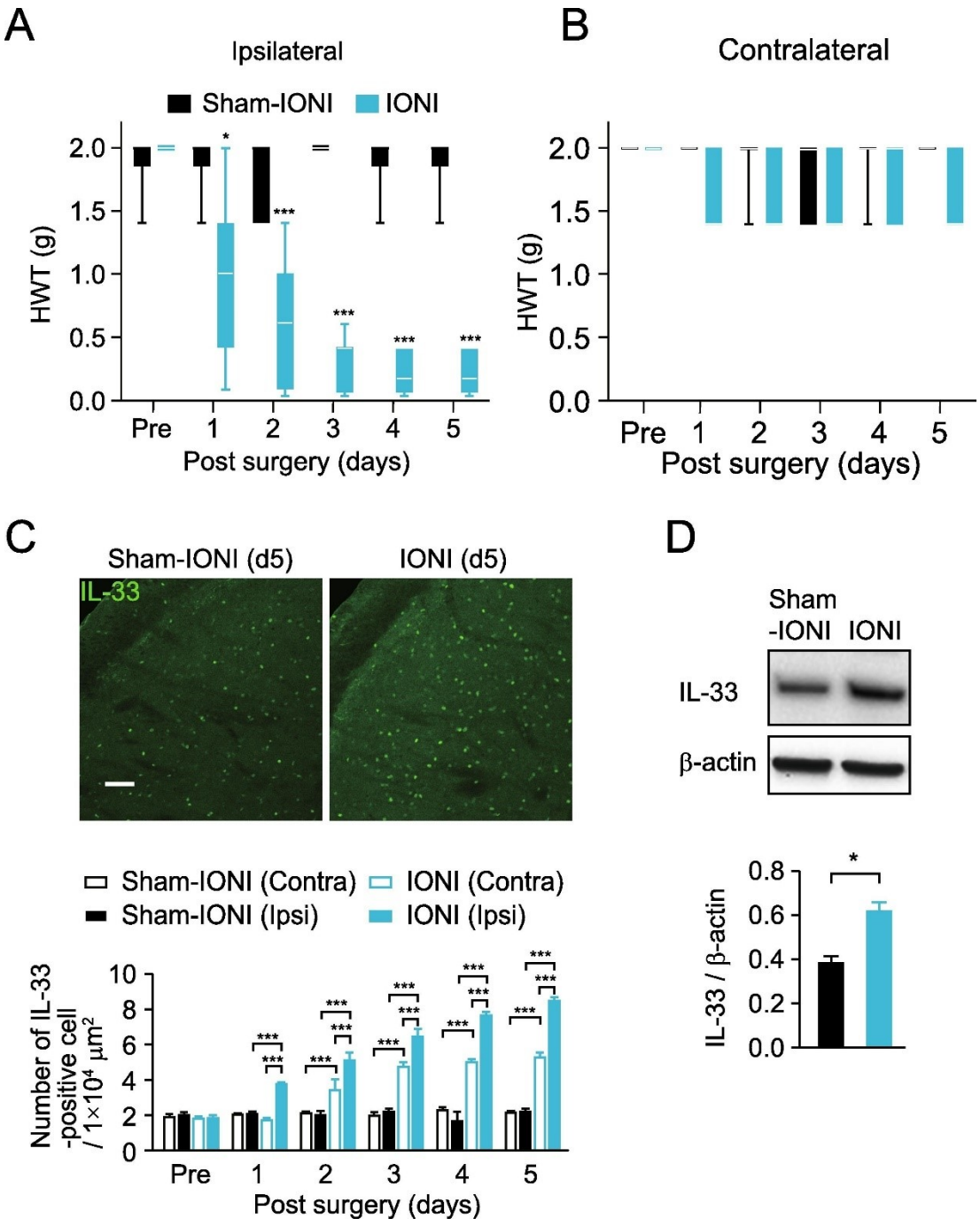

Figure 1. Orofacial mechanical allodynia and upregulation of IL-33 in the Vc following IONI. (A, B) Time course of HWT in the ipsilateral (A) and contralateral sides (B) of the whisker pad skin following IONI. n = 7 mice in each; GEE folloourd by Bonferroni's test, $P < 0.001$, df = 1, Wald chi-square = 114.16 (A); $P = 1.000$, df = 1, Wald chi-square = 0.000 (B), Sham-IONI vs. IONI. *$P < 0.05$, ***$P < 0.001$. Boxes show the 25th–75th percentiles with the median value indicated as a line within each box. Whiskers indicate the 10th and 90th percentiles of the data. (C) Representative images of IL-33 immunofluorescence in the ipsilateral side of the Vc of

sham-IONI and IONI mice on day 5 after surgery. Scale bar = 50 μm. The column represents the average number of IL-33-positive cells in the contralateral and ipsilateral sides of the Vc following sham-IONI or IONI. n = 3 mice in each; two-way ANOVA Tukey's multiple comparison test; ***$P < 0.001$. Data represent the mean ± SEM. (D) Representative blots of IL-33 expression in the ipsilateral side of the Vc of sham-IONI and IONI mice on day 5 after surgery. The column represents the average value of IL-33/β-actin. n = 4 mice in each; unpaired Student's *t*-test; * $P < 0.05$. Data represent the mean ± SEM.

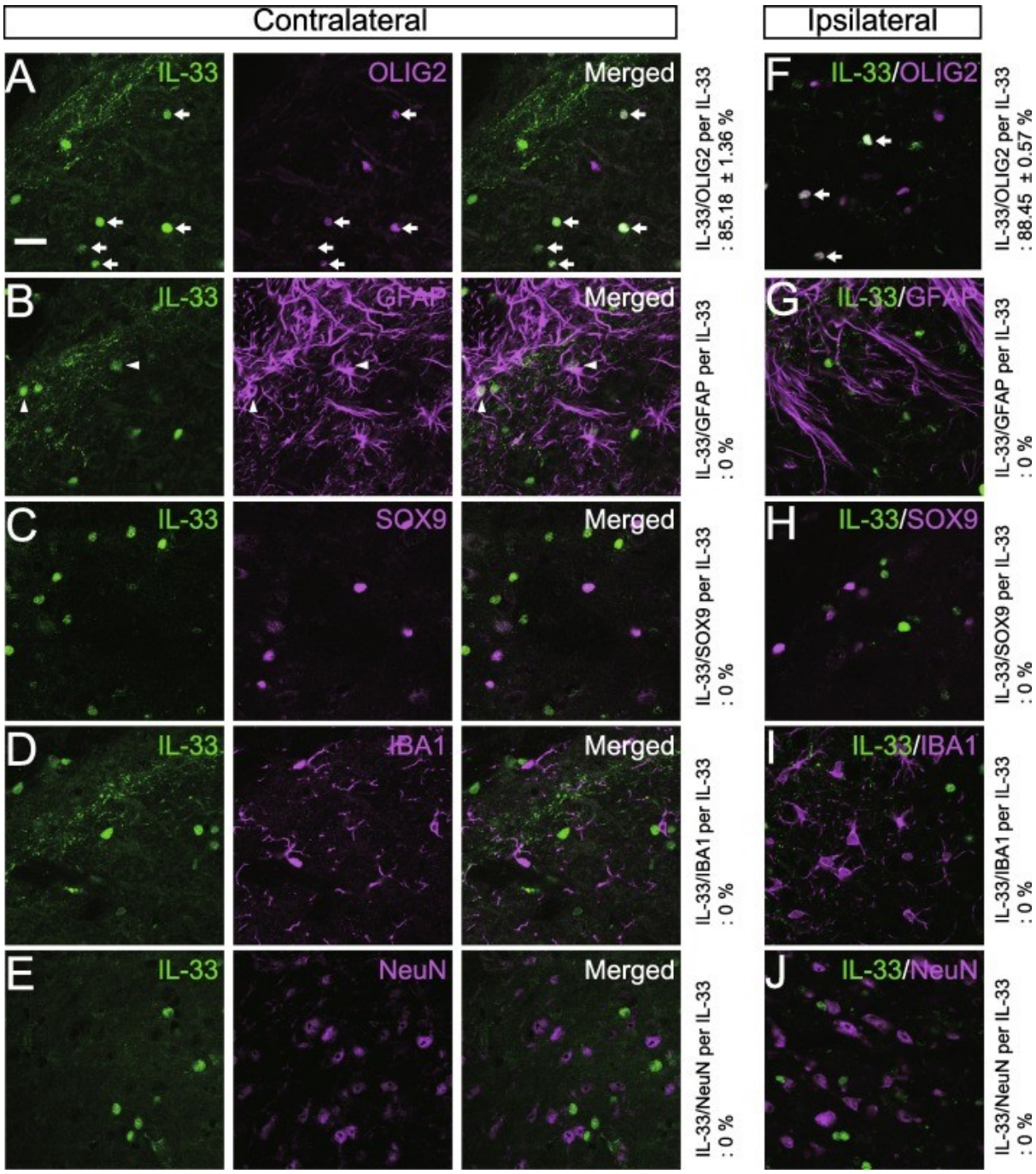

Figure 2. Expression patterns of IL-33 in the Vc. Representative images of IL-33 (green) and OLIG2, GFAP, SOX9, IBA1, or NeuN (magenta) immunofluorescence in the contralateral (A-E) and ipsilateral sides (F-J) of the Vc 5 days following IONI. Arrows indicate IL-33/OLIG2 double-positive cells. Arrowheads indicate IL-33-positive cells surrounded by GFAP immunofluorescence. Scale bar = 20 μm. The average ratio of cell markers + IL-33 per IL-33-positive cell is shown in the figure. n = 3 mice in each. Data represent the mean ± SEM.

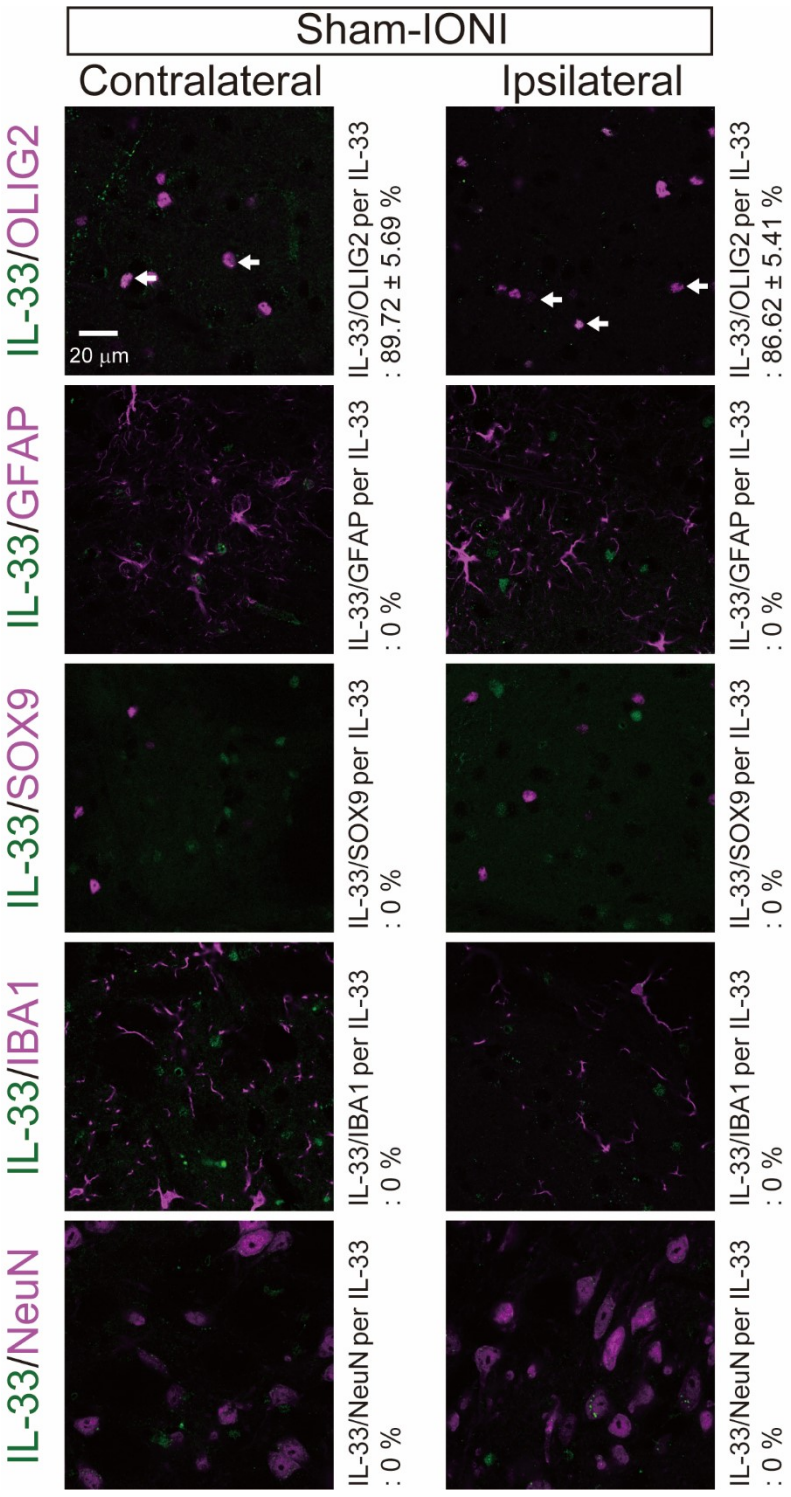

Figure 3. Expression patterns of IL-33 in the Vc. Representative images of IL-33 (green) and OLIG2, GFAP, SOX9, IBA1, or NeuN (magenta) immunofluorescence in the contralateral and ipsilateral sides of the Vc 5 days after Sham-IONI. Arrows indicate IL-33/OLIG2 double-positive cells. Scale bar = 20 μm. n = 3 mice in each. Data represent the mean ± SEM.

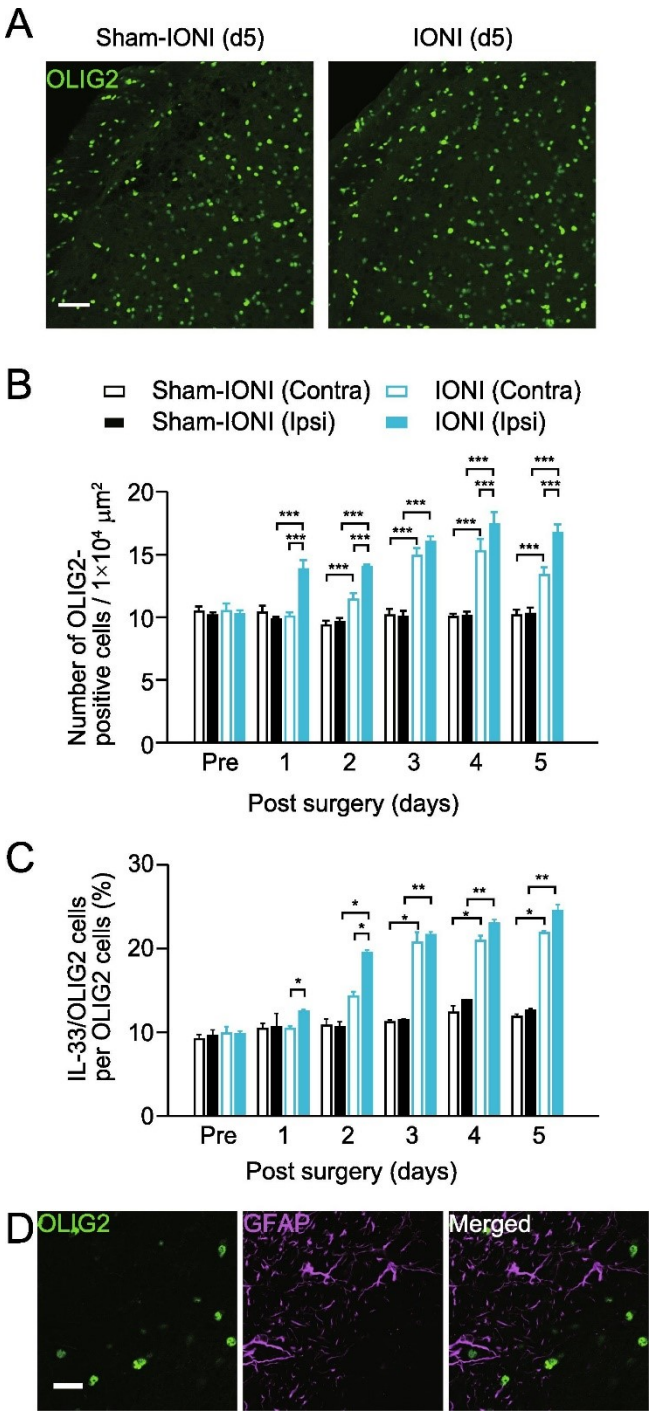

Figure 4. OLIG2-positive cells in the Vc after IONI. (A) Representative images of OLIG2-positive cells in the ipsilateral side of the Vc of sham-IONI and IONI mice on day 5 after surgery. Scale bar = 50 μm. (B) The column represents the average number of OLIG2-positive cells in the contralateral and ipsilateral sides of the Vc following sham-IONI or IONI. n = 3 mice in each; two-way ANOVA Tukey's multiple comparison test; ***$P < 0.001$. Data represent the mean ± SEM. (C) The column represents the average ratio of IL-33/OLIG2 double-positive

cells per OLIG2 positive cells in the contralateral and ipsilateral sides of the Vc following sham operation and IONI. n = 3 mice in each; two-way ANOVA Tukey's multiple comparison test; $*P < 0.05$, $**P < 0.01$. Data represent the mean ± SEM. (D) Representative double-staining image of OLIG2 and GFAP in the ipsilateral side of the Vc 5 days after IONI. Scale bar = 20 μm.

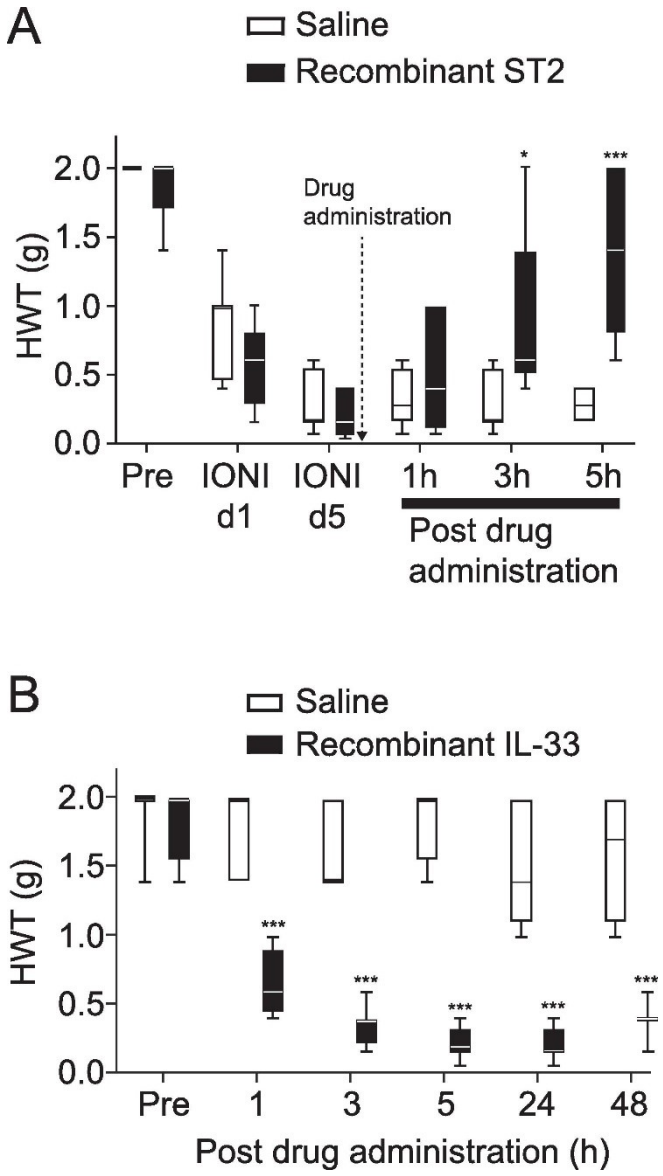

Figure 5. Requirement of IL-33 signaling in the Vc in mechanical allodynia. (A) Time course of HWT in IONI mice intracisternally administered with saline or recombinant ST2 on day 5 after IONI. n = 8 mice (Saline), n = 9 mice (Recombinant ST2). GEE followed by Bonferroni's test, $P < 0.05$, df = 1, Wald chi-square = 5.855, Saline vs. Recombinant ST2. *$P < 0.05$, ***$P < 0.001$. (B) Time course of HWT in naive mice intracisternally administered with saline or recombinant IL-33 n = 8 in each. GEE followed by Bonferroni's test, $P < 0.001$, df = 1, Wald chi-square = 202.453, Saline vs. Recombinant IL-33. ***$P < 0.001$. Boxes show the 25th–75th percentiles with the median value indicated as a line within each box. Whiskers indicate the 10th and 90th percentiles of the data.

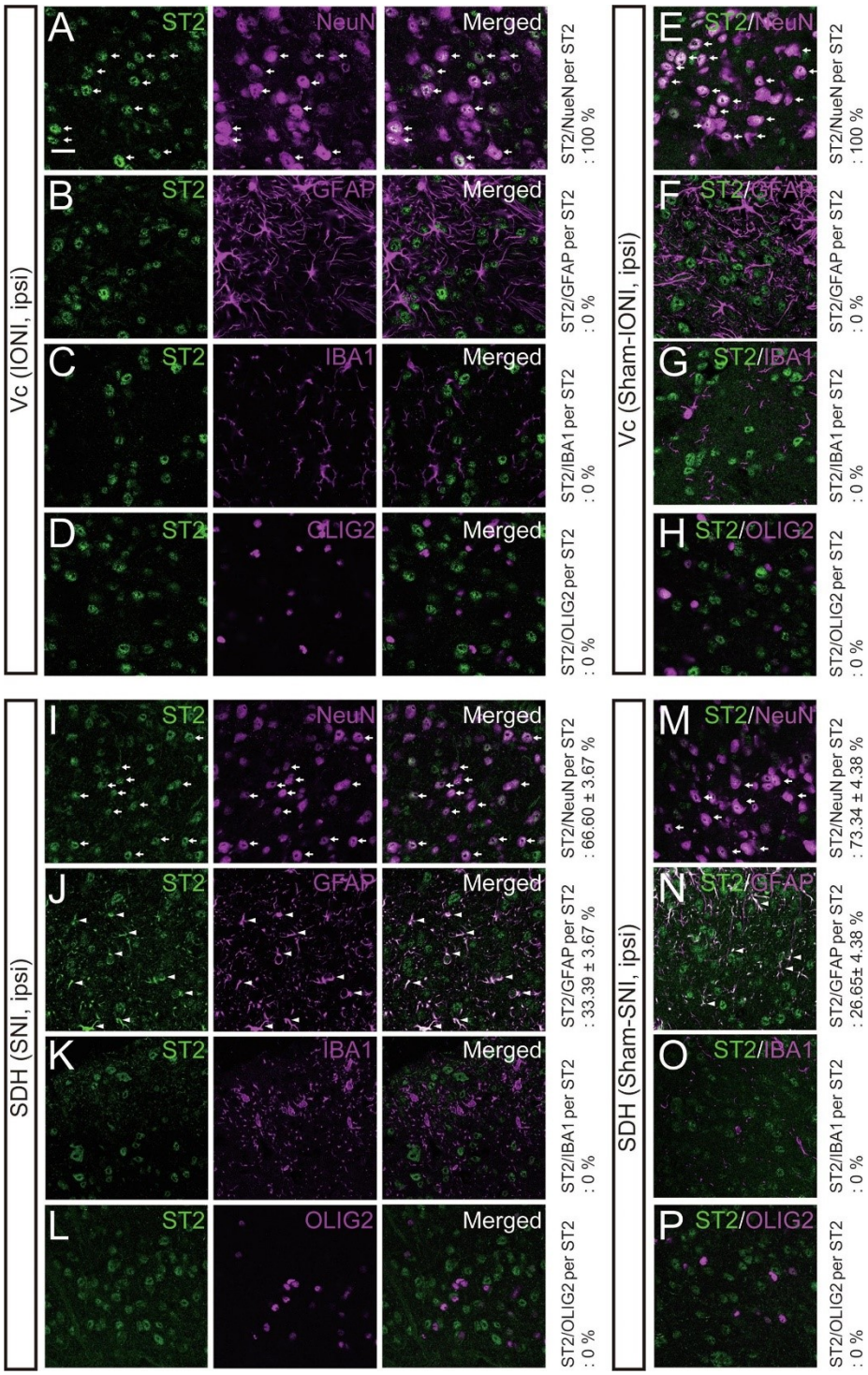

Figure 6. Expression patterns of ST2 in the Vc or SDH. (A-H) Representative images showing ST2 (green) and NeuN, GFAP, IBA1, or OLIG2 (magenta) immunofluorescence in the ipsilateral (A-D) and contralateral sides (E-H) of the Vc 5 days following IONI. (I-P) Representative images showing ST2 (green) and NeuN, GFAP, IBA1, or OLIG2 (magenta) immunofluorescence in the ipsilateral (I-L) and contralateral sides (M-P) of the SDH 5 days

following SNI. Arrows and arrowheads indicate ST2/NeuN and ST2/GFAP double-positive cells, respectively. Scale bar = 20 μm. The average ratio of cell markers + ST2 per ST2-positive cell is shown in the figure. n = 3 (IONI mice), n = 3 (SNI mice). Data represent the mean ± SEM.

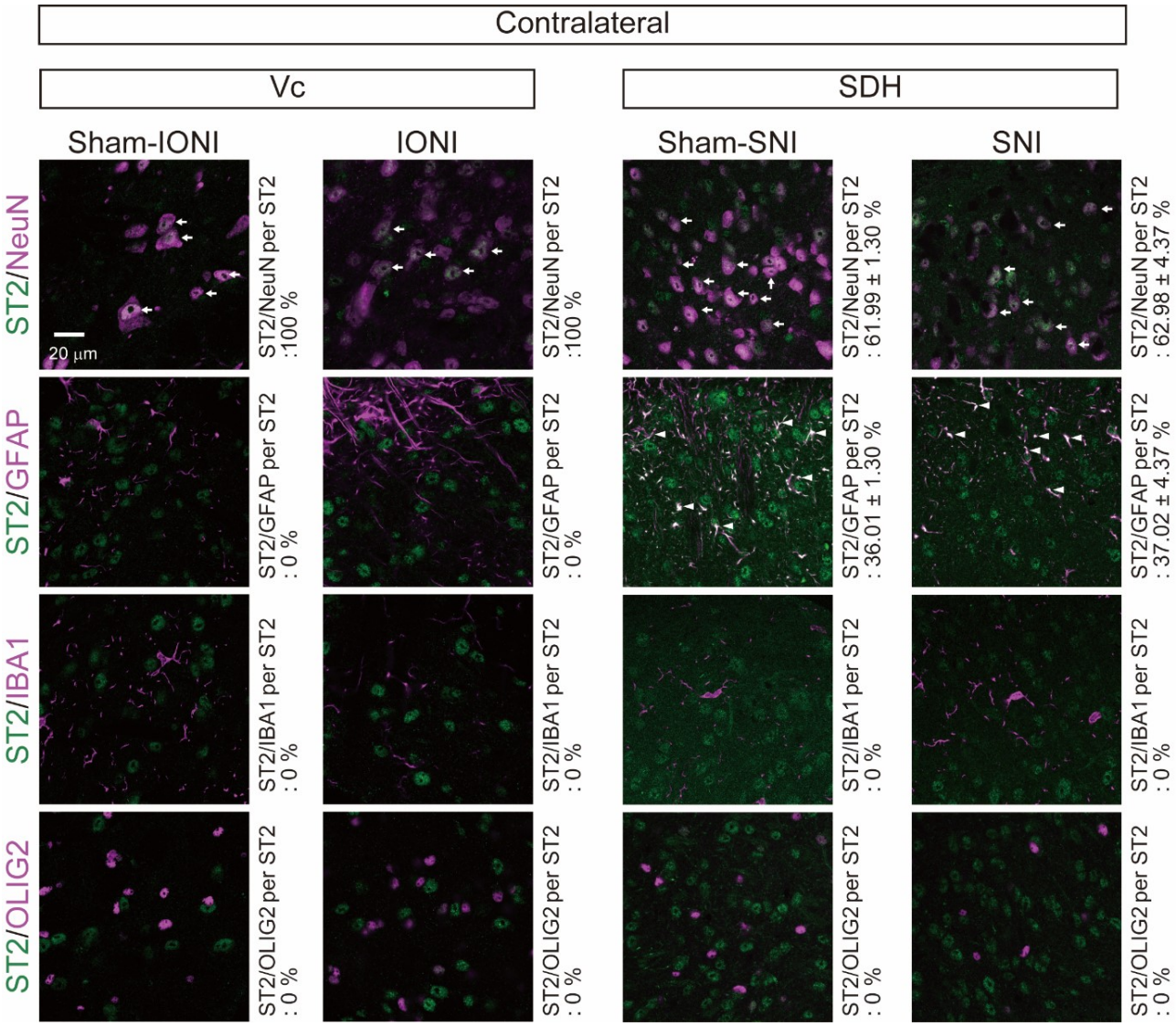
Contralateral
Vc
SDH
Sham-IONI
IONI
Sham-SNI
SNI
ST2/NeuN
ST2/GFAP
ST2/IBA1
ST2/OLIG2
20 μm
ST2/NeuN per ST2 :100 %
ST2/NeuN per ST2 :100 %
ST2/NeuN per ST2 : 61.99 ± 1.30 %
ST2/NeuN per ST2 : 62.98 ± 4.37 %
ST2/GFAP per ST2 : 0 %
ST2/GFAP per ST2 : 0 %
ST2/GFAP per ST2 : 36.01 ± 1.30 %
ST2/GFAP per ST2 : 37.02 ± 4.37 %
ST2/IBA1 per ST2 : 0 %
ST2/IBA1 per ST2 : 0 %
ST2/IBA1 per ST2 : 0 %
ST2/IBA1 per ST2 : 0 %
ST2/OLIG2 per ST2 : 0 %
ST2/OLIG2 per ST2 : 0 %
ST2/OLIG2 per ST2 : 0 %
ST2/OLIG2 per ST2 : 0 %

Figure 7. Expression patterns of ST2 in the Vc and SDH 5 days after nerve injury. Representative images of ST2 (green) and NeuN, GFAP, IBA1, and OLIG2 (magenta) immunofluorescence in the contralateral side of the Vc and SDH following IONI and SNI, respectively. Arrows and arrowheads indicate ST2/NeuN and ST2/GFAP double-positive cells, respectively. Scale bar = 20 μm. n = 3 mice in each. Data represent the mean ± SEM

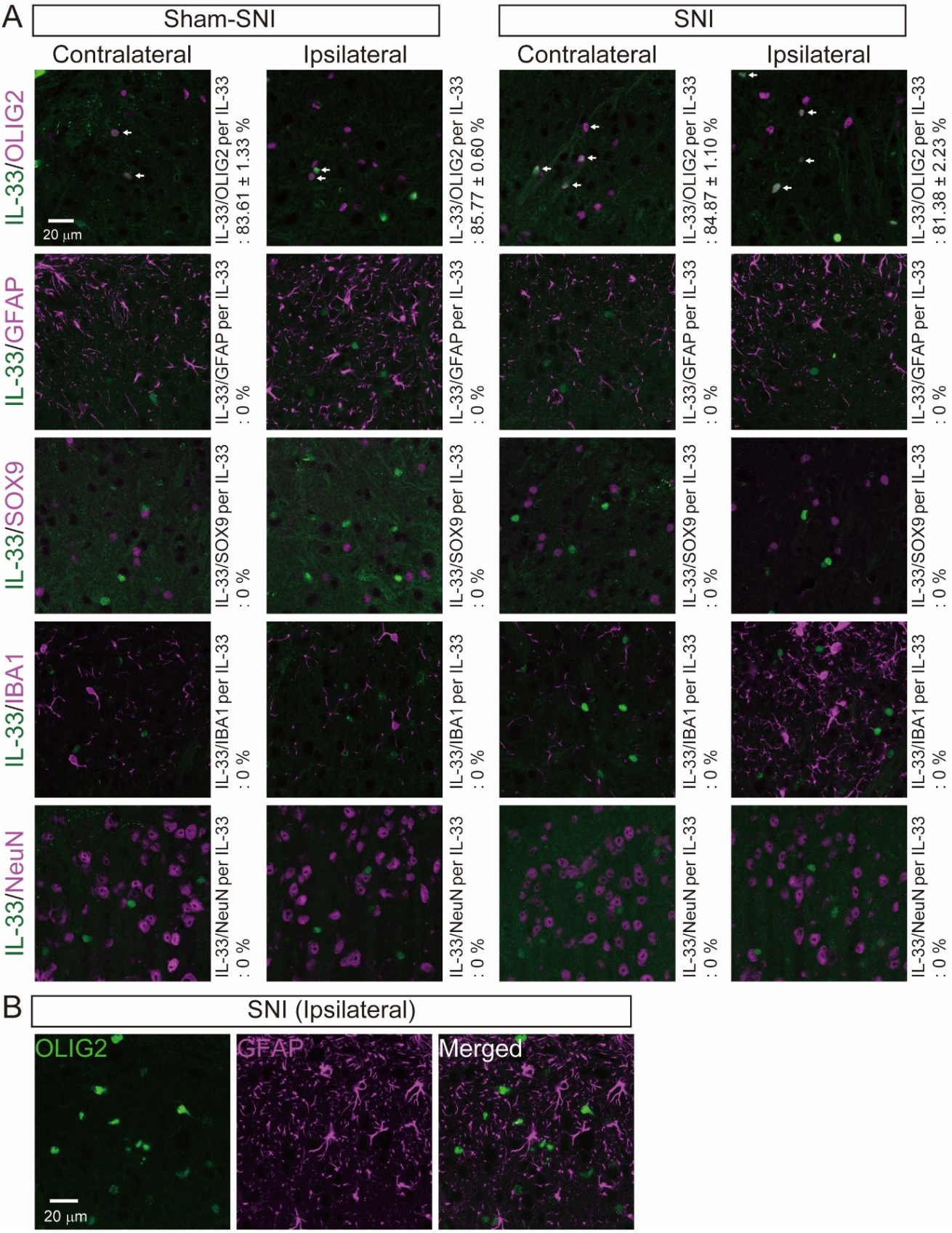
A
Sham-SNI
SNI
Contralateral
Ipsilateral
Contralateral
Ipsilateral
IL-33/OLIG2
IL-33/GFAP
IL-33/SOX9
IL-33/IBA1
IL-33/NeuN
20 μm
IL-33/OLIG2 per IL-33 : 83.61 ± 1.33 %
IL-33/OLIG2 per IL-33 : 85.77 ± 0.60 %
IL-33/OLIG2 per IL-33 : 84.87 ± 1.10 %
IL-33/OLIG2 per IL-33 : 81.38 ± 2.23 %
IL-33/GFAP per IL-33 : 0 %
IL-33/SOX9 per IL-33 : 0 %
IL-33/IBA1 per IL-33 : 0 %
IL-33/NeuN per IL-33 : 0 %
B
SNI (Ipsilateral)
OLIG2
GFAP
Merged
20 μm

Figure. 8. Expression patterns of IL-33 in the SDH 5 days after SNI. (A) Representative images of IL-33 (green) and OLIG2, GFAP, SOX9, IBA1, and NeuN (magenta) immunofluorescence in both contralateral and ipsilateral sides of the SDH of Sham-SNI and SNI mice. Arrows indicate IL-33/OLIG2 double-positive cells. Scale bar = 20 μm. n = 3 mice in each. Data represent the mean ± SEM. (B) Representative images showing OLIG2 (green) and GFAP (magenta) fluorescence in the SDH 5 days after SNI. Scale bar = 20 μm.

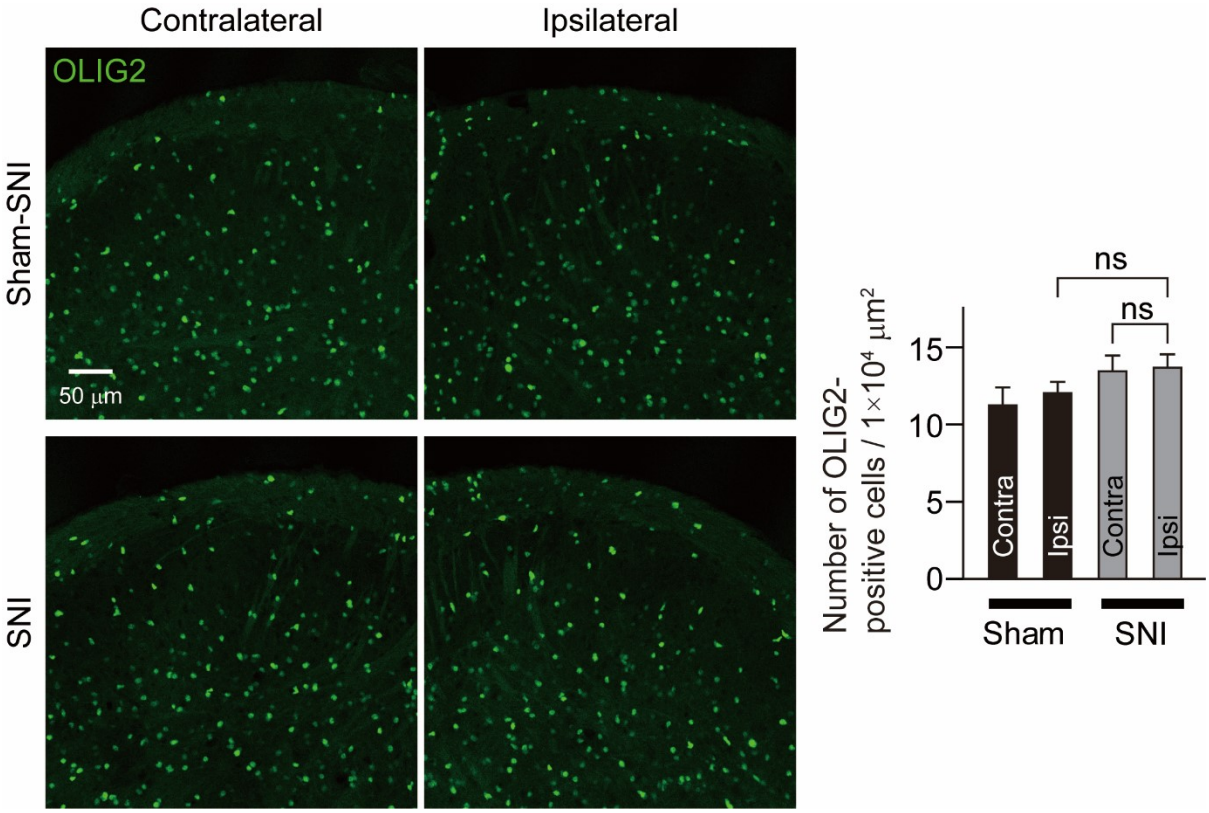

Figure. 9. Expression of OLIG2 in the SDH 5 days following SNI. Representative images showing OLIG2 (green) immunofluorescence in both contralateral and ipsilateral sides of the SDH of Sham-SNI and SNI mice. Scale bar = 50 μm. The average number of OLIG2 positive cells. n = 5 mice in each. Data represent the mean ± SEM. Unpaired Student's *t*-test; ns: not significant.

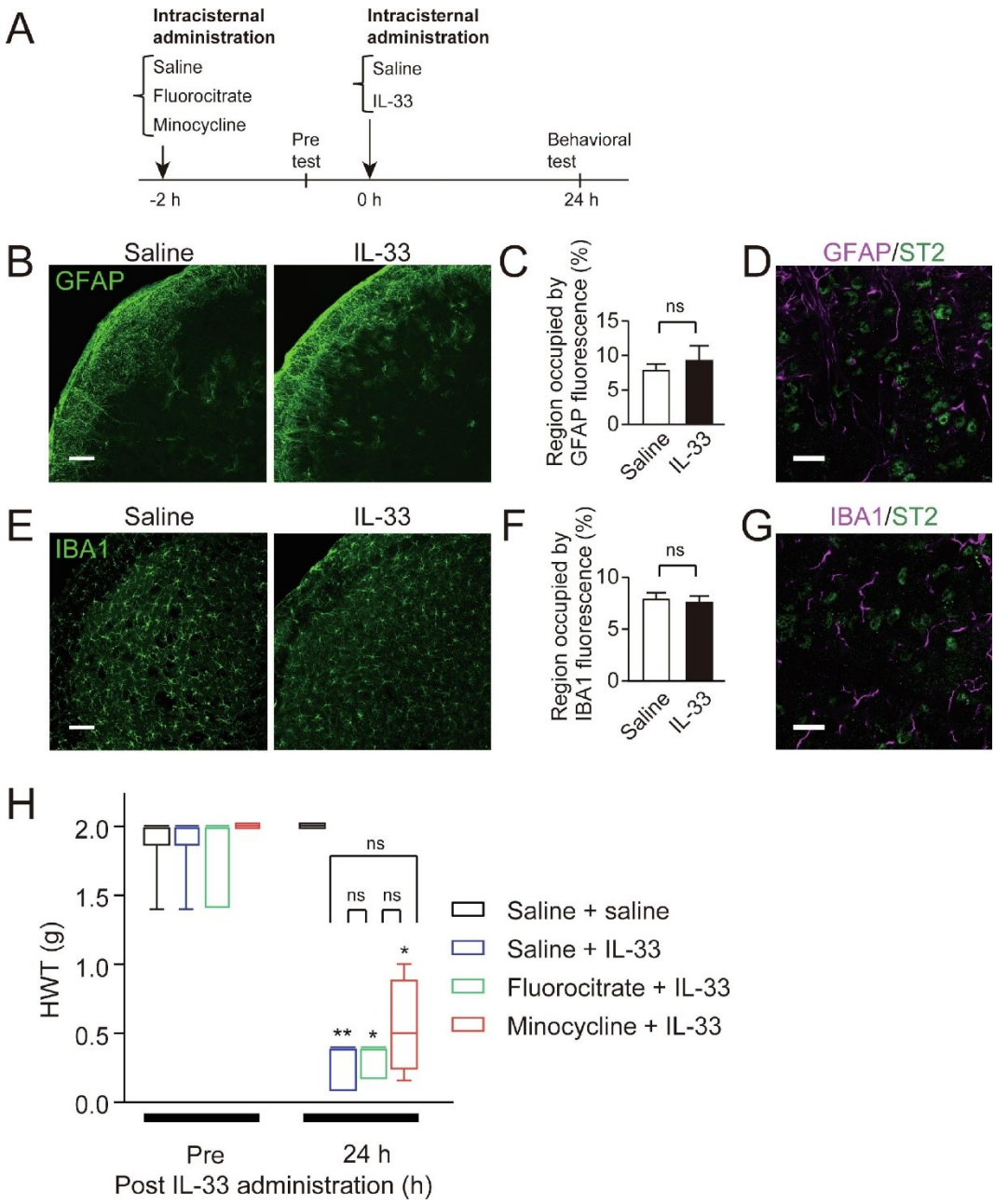

Figure 10. Glial cell expression patterns in the Vc and glial cell-independent IL-33-induced mechanical allodynia. (A) A timeline of the experimental schedule. (B-G) Immunohistochemical analyses of GFAP (B-D) and IBA1 (E-G) in the Vc 24 h after intracisternal administration of saline or IL-33 in naive mice. Representative images showing GFAP (B) and IBA1 (E) immunofluorescence in the Vc in saline or IL-33-administered mice. Scale bars = 100 μm. (C, F) Average values of the region occupied by GFAP (C) and IBA1 (F) immunofluorescence in the Vc. n = 6 mice (Saline), n = 5 mice (IL-33); unpaired Student's *t*-test; ns: not significant. Data represent the mean ± SEM. (D, G) Representative images showing GFAP/ST2 (D) and IBA1/ST2 (G) immunofluorescence in the Vc of IL-33-administered mice.

Scale bars = 20 μm. (H) Effects of minocycline or fluorocitrate on IL-33-induced mechanical allodynia. Fluorocitrate or minocycline was administered intracisternally 2 h prior to IL-33 administration. n = 6 mice (Saline + saline), n = 6 mice (Saline + IL-33), n = 5 mice (Minocycline + IL-33), and n = 4 mice (Fluorocitrate + IL-33); Kruskal-Wallis Dunn's multiple comparison test, $^{*}P < 0.05$, $^{**}P < 0.01$ vs. Saline (24 h); ns: not significant. Boxes show the 25th–75th percentiles with the median value indicated as a line within each box. Whiskers indicate the 10th and 90th percentiles of the data.

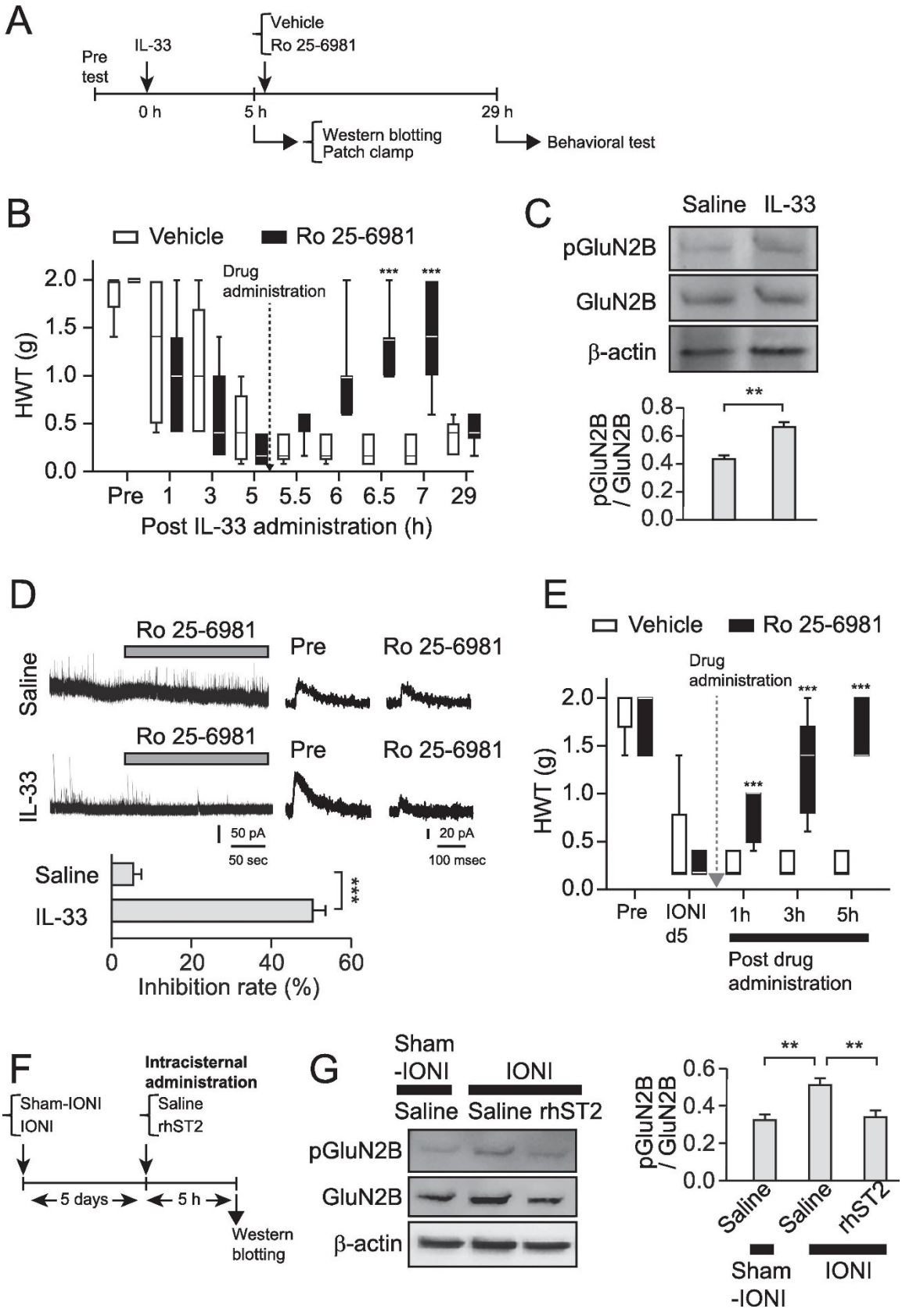
A
Pre test
IL-33
Vehicle
Ro 25-6981
0 h
5 h
29 h
Western blotting
Patch clamp
Behavioral test
B
Vehicle
Ro 25-6981
Drug administration
HWT (g)
Pre 1 3 5 5.5 6 6.5 7 29
Post IL-33 administration (h)
C
Saline IL-33
pGluN2B
GluN2B
β-actin
pGluN2B / GluN2B
D
Ro 25-6981
Pre
Saline
IL-33
50 pA
50 sec
20 pA
100 msec
Inhibition rate (%)
E
Vehicle
Ro 25-6981
Drug administration
HWT (g)
Pre
IONI d5
1h
3h
5h
Post drug administration
F
Intracisternal administration
Sham-IONI
IONI
Saline
rhST2
5 days
5 h
Western blotting
G
Sham -IONI
IONI
Saline Saline rhST2
pGluN2B
GluN2B
β-actin
pGluN2B / GluN2B
Saline
Saline
rhST2
Sham -IONI
IONI

Figure 11. GluN2B activation in Vc neurons following intracisternal administration of IL-33. (A) A timeline of the experimental schedule. (B) Effect of Ro 25-6981 on IL-33-induced mechanical allodynia. n = 5 mice (Vehicle), n = 7 mice (Ro 25-6981). GEE followed by Bonferroni's test, $P < 0.05$, df = 1, Wald chi-square = 4.261, Vehicle vs. Ro 25-6981. ***$P < 0.001$. Boxes show the 25th–75th percentiles with the median value indicated as a line within each box. Whiskers indicate the 10th and 90th percentiles of the data. (C) Representative blot of phosphorylated-GluN2B (pGluN2B) expression in the synaptosomal fraction in the Vc prepared 5 h after intracisternal administration of saline or IL-33. The column represents the average value of pGluN2B/GluN2B. n = 5 mice in each; unpaired Student's *t*-test; ** $P < 0.01$. (D) Representative full traces (left panel) and single events (right panel) of mEPSC in Vc neurons of saline- or IL-33-administered mice. Calibration bars indicate 50 pA and 50 sec (left panels) and 20 pA and 100 msec (right panels). Ro 25-6981 was continuously applied during the gray bar-indicated period. The column represents the average value of inhibition rate of mEPSC by Ro 25-6981. n = 16 neurons from 4 mice for saline, n = 18 neurons from 4 mice for IL-33; unpaired Student's *t*-test; *** $P < 0.001$. (E) Effect of Ro 25-6981 on mechanical allodynia following IONI. n = 5 mice in each. GEE followed by Bonferroni's test, $P < 0.001$, df = 1, Wald chi-square = 29.623, Vehicle vs. Ro 25-6981. ***$P < 0.001$. Boxes show the 25th–75th percentiles with the median value indicated as a line within each box. Whiskers indicate the 10th and 90th percentiles of the data. (F) A timeline of the experimental schedule. (G) Representative blot of pGluN2B levels in the synaptosomal fraction in the Vc prepared 5 h after intracisternal administration of saline or rhST2 on day 5 in IONI mice. The column represents the average value of pGluN2B/GluN2B. n = 5 mice in each; one-way ANOVA Tukey's test; ** $P < 0.01$. Data represent the mean ± SEM.

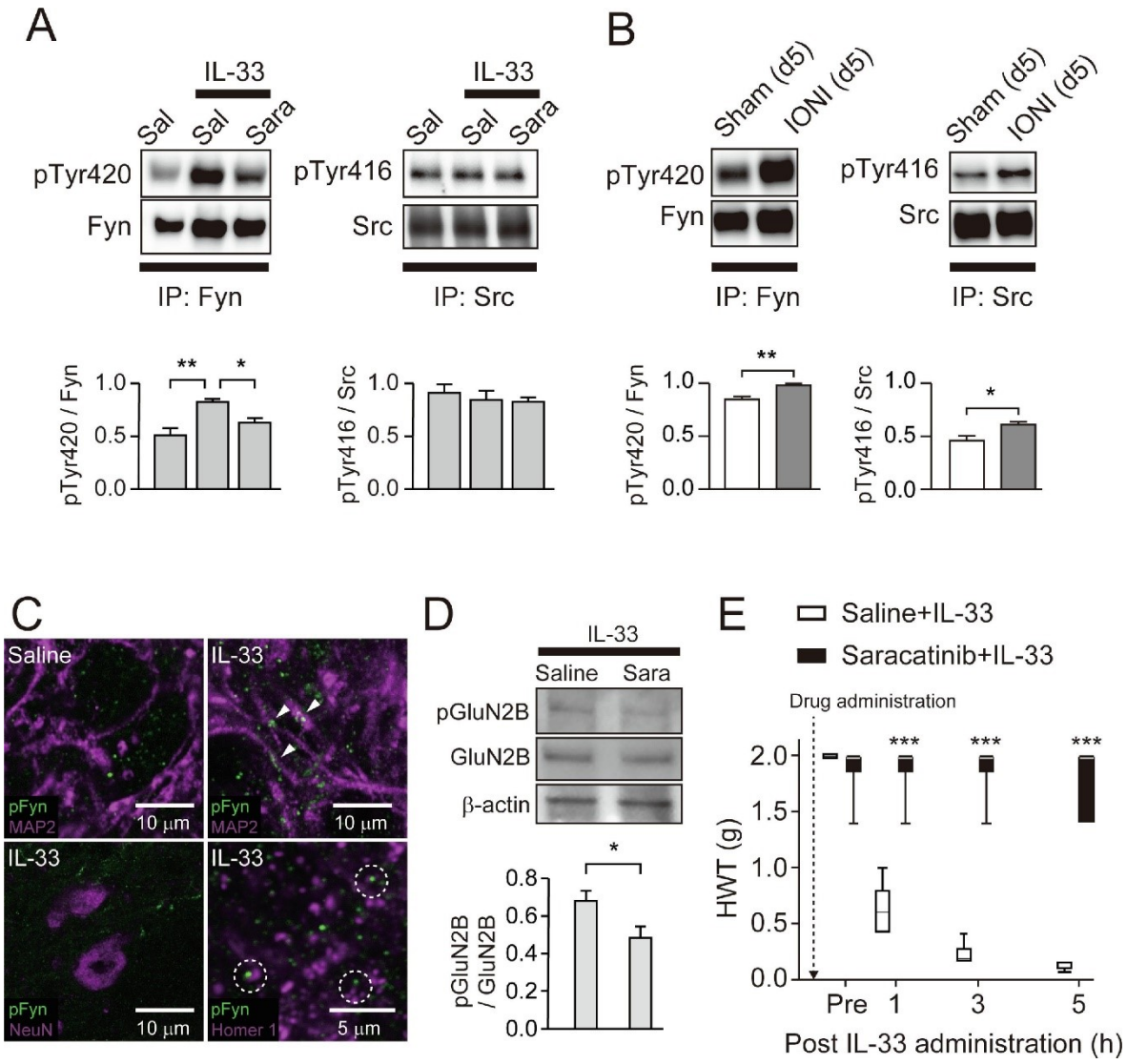

Figure 12. IL-33-mediated phosphorylation of GluN2B via Fyn kinase. (A) Representative blots of phosphorylated-Tyr420 (pTyr420) and phosphorylated-Tyr416 (pTyr416) levels in the whole fraction of the Vc 5 h after intracisternal administration of saline or IL-33. Saline (Sal) or saracatinib (Sara) administered 2 h prior to IL-33 administration. The column represents the average value of pTyr420/Fyn or pTyr416/Src. n = 5 mice in each; one-way ANOVA Tukey's test; * $P < 0.05$, ** $P < 0.01$. Data represent the mean ± SEM. (B) Representative blots of pTyr420 and pTyr416 levels in the whole fraction of the ipsilateral side of the Vc 5 d after surgery. n = 5 mice in each; unpaired Student's *t*-test; * $P < 0.05$, ** $P < 0.01$. Data represent the mean ± SEM. (C) Representative images showing pFyn (green) and MAP2, NeuN, or Homer 1 (magenta) expression in the Vc 5 days after saline or IL-33 administration. Arrowheads indicate pFyn puncta on the dendritic shaft. Circles indicate the regions where pFyn puncta are in contact with Homer 1 puncta. (D) Representative blots of pGluN2B

expression in a synaptosomal fraction of the Vc 5 h after intracisternal administration of IL-33 with pretreatment of saline or saracatinib. The column represents the average value of pGluN2B/GluN2B. n = 5 mice in each; unpaired Student's *t*-test; * $P < 0.05$. Data represent the mean ± SEM. (E) Effect of saracatinib on IL-33-induced mechanical allodynia. n = 5 mice (Saline + IL-33), n = 6 mice (Saracatinib + IL-33). GEE followed by Bonferroni's test, $P < 0.001$, df = 1, Wald chi-square = 406.309, Saline + IL-33 vs. Saracatinib + IL-33. ***$P < 0.001$. Boxes show the 25th–75th percentiles with the median value indicated as a line within each box. Whiskers indicate the 10th and 90th percentiles of the data.

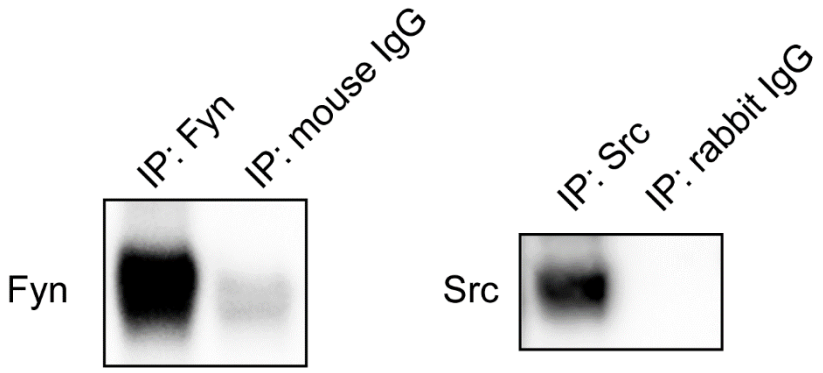

Figure 13. Representative blots of Fyn and Src levels in the Vc of naïve mice. Whole-cell lysates were immunoprecipitated with Fyn, mouse IgG (control for Fyn), Src, or rabbit IgG (control for Src). Bands were detected by anti-Fyn or anti-Src antibodies

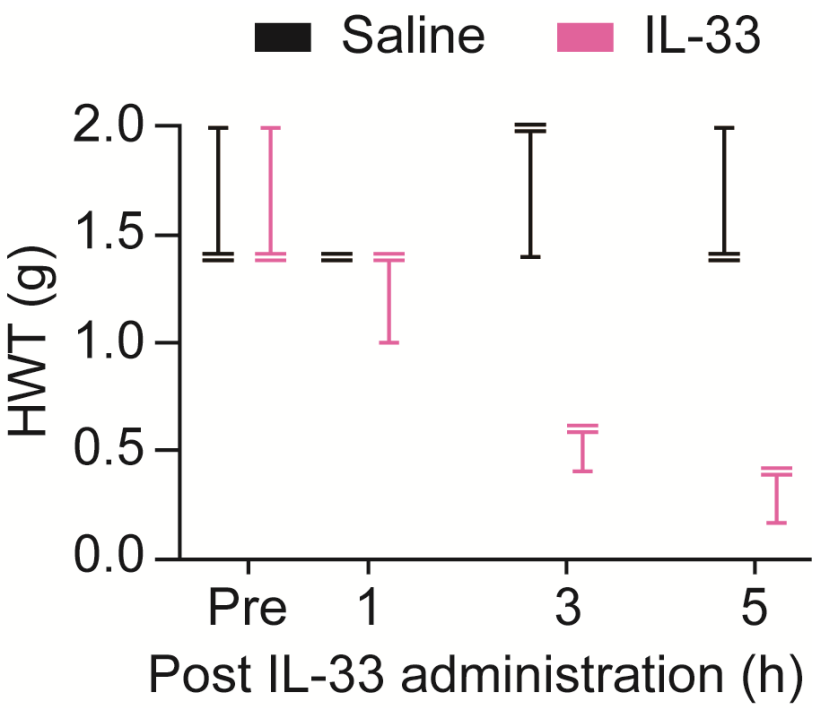

Figure.14 Time course of the HWT in naive mice that received an intracisternal administration of saline or recombinant IL-33. n = 3 mice in each. Boxes show the 25th–75th percentiles with the median value indicated as a line within each box. Whiskers indicate the 10th and 90th percentiles of the data. (P = 0.000, GEE Wald chi-square = 49.830; Fig. 9G).

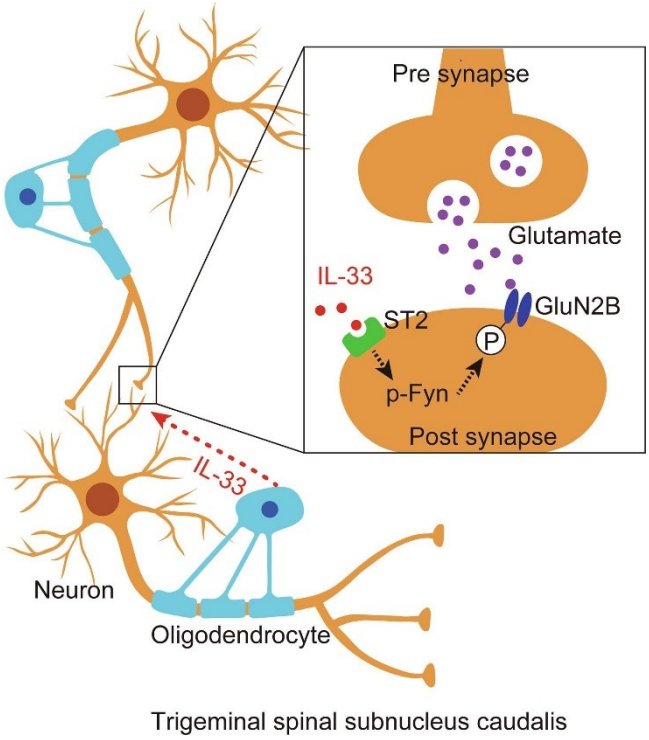

Figure. 15 A schematic illustration of the proposed model of orofacial neuropathic pain. After IONI, the number of oligodendrocytes increases in the Vc and they secrete IL-33. Activation of ST2 in Vc neurons causes phosphorylation of Fyn kinase and subsequent phosphorylation of GluN2B. Thereby, excitatory neurotransmission in the Vc is potentiated, culminating in the development of orofacial neuropathic pain.